

Wireless Network Models Using Graphs

Lead Guest Editor: Jose M. Gimenez-Guzman

Guest Editors: R. Maheswar, Kaharudin Dimiyati, and Ivan Marsa-Maestre





Wireless Network Models Using Graphs

Wireless Communications and Mobile Computing

Wireless Network Models Using Graphs

Lead Guest Editor: Jose M. Gimenez-Guzman


Guest Editors: R. Maheswar, Kaharudin Dimiyati,
and Ivan Marsa-Maestre




Copyright © 2022 Hindawi Limited. All rights reserved.

This is a special issue published in “Wireless Communications and Mobile Computing.” All articles are open access articles distributed under the Creative Commons Attribution License, which permits unrestricted use, distribution, and reproduction in any medium, provided the original work is properly cited.

Chief Editor

Zhipeng Cai , USA

Associate Editors

Ke Guan , China
Jaime Lloret , Spain
Maode Ma , Singapore

Academic Editors

Muhammad Inam Abbasi, Malaysia
Ghufran Ahmed , Pakistan
Hamza Mohammed Ridha Al-Khafaji ,
Iraq
Abdullah Alamoodi , Malaysia
Marica Amadeo, Italy
Sandhya Aneja, USA
Mohd Dilshad Ansari, India
Eva Antonino-Daviu , Spain
Mehmet Emin Aydin, United Kingdom
Parameshchhari B. D. , India
Kalapaveen Bagadi , India
Ashish Bagwari , India
Dr. Abdul Basit , Pakistan
Alessandro Bazzi , Italy
Zdenek Becvar , Czech Republic
Nabil Benamar , Morocco
Olivier Berder, France
Petros S. Bithas, Greece
Dario Bruneo , Italy
Jun Cai, Canada
Xuesong Cai, Denmark
Gerardo Canfora , Italy
Rolando Carrasco, United Kingdom
Vicente Casares-Giner , Spain
Brijesh Chaurasia, India
Lin Chen , France
Xianfu Chen , Finland
Hui Cheng , United Kingdom
Hsin-Hung Cho, Taiwan
Ernestina Cianca , Italy
Marta Cimitile , Italy
Riccardo Colella , Italy
Mario Collotta , Italy
Massimo Condoluci , Sweden
Antonino Crivello , Italy
Antonio De Domenico , France
Floriano De Rango , Italy






Antonio De la Oliva , Spain
Margot Deruyck, Belgium
Liang Dong , USA
Praveen Kumar Donta, Austria
Zhuojun Duan, USA
Mohammed El-Hajjar , United Kingdom
Oscar Esparza , Spain
Maria Fazio , Italy
Mauro Femminella , Italy
Manuel Fernandez-Veiga , Spain
Gianluigi Ferrari , Italy
Luca Foschini , Italy
Alexandros G. Fragkiadakis , Greece
Ivan Ganchev , Bulgaria
Óscar García, Spain
Manuel García Sánchez , Spain
L. J. García Villalba , Spain
Miguel Garcia-Pineda , Spain
Piedad Garrido , Spain
Michele Girolami, Italy
Mariusz Glabowski , Poland
Carles Gomez , Spain
Antonio Guerrieri , Italy
Barbara Guidi , Italy
Rami Hamdi, Qatar
Tao Han, USA
Sherief Hashima , Egypt
Mahmoud Hassaballah , Egypt
Yejun He , China
Yixin He, China
Andrej Hrovat , Slovenia
Chunqiang Hu , China
Xuexian Hu , China
Zhenghua Huang , China
Xiaohong Jiang , Japan
Vicente Julian , Spain
Rajesh Kaluri , India
Dimitrios Katsaros, Greece
Muhammad Asghar Khan, Pakistan
Rahim Khan , Pakistan
Ahmed Khattab, Egypt
Hasan Ali Khattak, Pakistan
Mario Kolberg , United Kingdom
Meet Kumari, India
Wen-Cheng Lai , Taiwan

Jose M. Lanza-Gutierrez, Spain
Pavlos I. Lazaridis , United Kingdom
Kim-Hung Le , Vietnam
Tuan Anh Le , United Kingdom
Xianfu Lei, China
Jianfeng Li , China
Xiangxue Li , China
Yaguang Lin , China
Zhi Lin , China
Liu Liu , China
Mingqian Liu , China
Zhi Liu, Japan
Miguel López-Benítez , United Kingdom
Chuanwen Luo , China
Lu Lv, China
Basem M. ElHalawany , Egypt
Imadeldin Mahgoub , USA
Rajesh Manoharan , India
Davide Mattera , Italy
Michael McGuire , Canada
Weizhi Meng , Denmark
Klaus Moessner , United Kingdom
Simone Morosi , Italy
Amrit Mukherjee, Czech Republic
Shahid Mumtaz , Portugal
Giovanni Nardini , Italy
Tuan M. Nguyen , Vietnam
Petros Nicolitidis , Greece
Rajendran Parthiban , Malaysia
Giovanni Pau , Italy
Matteo Petracca , Italy
Marco Picone , Italy
Daniele Pinchera , Italy
Giuseppe Piro , Italy
Javier Prieto , Spain
Umair Rafique, Finland
Maheswar Rajagopal , India
Sujan Rajbhandari , United Kingdom
Rajib Rana, Australia
Luca Reggiani , Italy
Daniel G. Reina , Spain
Bo Rong , Canada
Mangal Sain , Republic of Korea
Praneet Saurabh , India

Hans Schotten, Germany
Patrick Seeling , USA
Muhammad Shafiq , China
Zaffar Ahmed Shaikh , Pakistan
Vishal Sharma , United Kingdom
Kaize Shi , Australia
Chakchai So-In, Thailand
Enrique Stevens-Navarro , Mexico
Sangeetha Subbaraj , India
Tien-Wen Sung, Taiwan
Suhua Tang , Japan
Pan Tang , China
Pierre-Martin Tardif , Canada
Sreenath Reddy Thummaluru, India
Tran Trung Duy , Vietnam
Fan-Hsun Tseng, Taiwan
S Velliangiri , India
Quoc-Tuan Vien , United Kingdom
Enrico M. Vitucci , Italy
Shaohua Wan , China
Dawei Wang, China
Huaqun Wang , China
Pengfei Wang , China
Dapeng Wu , China
Huaming Wu , China
Ding Xu , China
YAN YAO , China
Jie Yang, USA
Long Yang , China
Qiang Ye , Canada
Changyan Yi , China
Ya-Ju Yu , Taiwan
Marat V. Yuldashev , Finland
Sherali Zeadally, USA
Hong-Hai Zhang, USA
Jiliang Zhang, China
Lei Zhang, Spain
Wence Zhang , China
Yushu Zhang, China
Kechen Zheng, China
Fuhui Zhou , USA
Meiling Zhu, United Kingdom
Zhengyu Zhu , China



Contents

On the Benefits of Channel Bonding in Dense, Decentralized Wi-Fi 4 Networks

Jose Manuel Gimenez-Guzman , Ivan Marsa-Maestre , David Orden , Susel Fernandez , and Marino Tejedor-Romero 

Research Article (11 pages), Article ID 8497585, Volume 2022 (2022)

Signal Propagation Models in Soil Medium for the Study of Wireless Underground Sensor Networks: A Review of Current Trends

Frank Kataka Banaseka , Ferdinand Katsriku, Jamal Deen Abdulai, Kofi Sarpong Adu-Manu , and Felicia Nana Ama Engmann 

Review Article (12 pages), Article ID 8836426, Volume 2021 (2021)

Optimal Sensor Placement for Underground Tunnel Monitoring via Wireless Sensor Networks

Yonggang Li , Bin He, and Youming Wang

Research Article (8 pages), Article ID 6621987, Volume 2021 (2021)

Research Article

On the Benefits of Channel Bonding in Dense, Decentralized Wi-Fi 4 Networks

Jose Manuel Gimenez-Guzman ¹, Ivan Marsa-Maestre ², David Orden ³,
Susel Fernandez ² and Marino Tejedor-Romero ³

¹Communications Department, Universitat Politècnica de València, Valencia, Spain

²Computer Engineering Department, Universidad de Alcalá, Alcalá de Henares, Spain

³Department of Physics and Mathematics, Universidad de Alcalá, Alcalá de Henares, Spain

Correspondence should be addressed to Jose Manuel Gimenez-Guzman; jmgimenez@upv.es

Received 7 July 2021; Revised 24 November 2021; Accepted 21 January 2022; Published 10 February 2022

Academic Editor: Ernestina Cianca

Copyright © 2022 Jose Manuel Gimenez-Guzman et al. This is an open access article distributed under the Creative Commons Attribution License, which permits unrestricted use, distribution, and reproduction in any medium, provided the original work is properly cited.

Channel bonding is a technique first defined in the IEEE 802.11n standard to increase the throughput in wireless networks by means of using wider channels. In IEEE 802.11n (nowadays also known as Wi-Fi 4), it is possible to use 40 MHz channels instead of the classical 20 MHz channels. Although using channel bonding can increase the throughput, the classic 802.11 setting only allows for two orthogonal channels in the 2.4 GHz frequency band, which is not enough for proper channel assignment in dense settings. For that reason, it is commonly accepted that channel bonding is not suitable for this frequency band. However, to the best of our knowledge, there is not any accurate study that deals with this issue thoroughly. In this work, we study in depth the effect of channel bonding in Wi-Fi 4 dense, decentralized networks operating in the 2.4 GHz frequency band. We confirm the negative effect of using channel bonding in the 2.4 GHz frequency band with 11 channels which are 20 MHz wide (as in North America), but we also show that when there are 13 or more channels at hand (as in many other parts of the world, including Europe and Japan), the use of channel bonding yields consistent throughput improvements. For that reason, we claim that the common assumption of not considering channel bonding in the 2.4 GHz band should be revised.

1. Introduction and State of the Art

The huge increase of wireless devices competing for the limited wireless bandwidth [1] has attracted the attention of researchers, since it is an increasingly complex problem. Especially in the case of the 2.4 GHz band, where a greater number of devices and protocols coexist, and in dense, decentralized settings such as residential buildings, we find very inefficient bandwidth usage situations [2]. The community is addressing this challenge in a twofold manner. Some researchers focus on new standards and specifications for high-efficiency wireless local area networks (HEWs) [2]. Others, however, focus on improving the centralized or decentralized coordination of devices and networks using the existing standards.

In the latter case, channel assignment techniques aim to optimize the distribution of channels among the transmitting devices, thus decreasing interference and increasing throughput [3–8]. An additional possibility, which exists since the IEEE 802.11n standard (Wi-Fi 4), is the use of *channel bonding*, which consists of using channels that are wider than the standard 20 MHz to achieve higher performance (higher bandwidth would allow for higher transmission rates, thus increasing throughput). A number of channel bonding techniques have been proposed in the literature for the different IEEE 802.11 standards [9–11]. We are especially interested in the standard IEEE 802.11n in the 2.4 GHz band. However, the general consensus is that using channel bonding in the 2.4 GHz band is not beneficial, since the interference due to the use of wider overlapping channels

jeopardizes the theoretical advantage of having higher maximum bit rates [12]. Consequently, most studies assume other bands such as the 5 GHz band [13–16], and the more recent ones generally assume dynamic channel bonding schemes for the 802.11ax standard [11,17].

Nevertheless, in our opinion, the possibilities of static channel bonding in the 802.11n 2.4 GHz have not been properly analyzed in the literature. Since most of the papers mentioning the limitations of channel bonding in this band directly focus on other bands or technologies (i.e., the 2.4 GHz band is not the focus of the paper), they either state these limitations as a matter of fact, not citing any study to back up the claim [18] or cite other papers which, in turn, state such limitations without the backup of an academic study [12,15,16,19]. There are some references to industrial white papers such as [20], but there the North American 11-channel 802.11 spectrum is assumed, although there are many regions in the world (e.g., Europe or Japan) where more channels are available. Furthermore, some studies directly assume the use of orthogonal channels, and therefore they do not consider interferences between adjacent channels [21], or they use only one wireless station (STA) per access point (AP) [10], while it has been shown that both interference between adjacent channels and STA number and precise placement may have a significant effect on throughput [22]. Taking this into account, we believe that the aforementioned consensus about the goodness of channel bonding in the 2.4 GHz band should be revised, as it is based on former studies [23–25] that concluded that channel bonding causes more harmful problems than it solves but these studies do not represent the density of current Wi-Fi networks.

In this paper, we study the effect of channel bonding in dense, decentralized Wi-Fi 4 scenarios, such as a residential building. The paper contributions can be summarized as follows:

- (i) We describe a graph-based scenario model for Wi-Fi 4 dense decentralized networks, using realistic indoor signal propagation and interference models, as well as the precise location and interference between all wireless devices (both access points (APs) and stations (STAs)), in order to compute the throughput. To the best of our knowledge, this is the first time that such an accurate model is used in the context of channel bonding (Section 2).
- (ii) We provide a three-dimensional realistic setting for a decentralized Wi-Fi 4 deployment in a residential building. For this setting, we generate 60 scenarios for different STA densities and placements (Section 2.1).
- (iii) We conduct an in-depth evaluation with the aforementioned model and setting, first for the classic 11-channel Wi-Fi 4 settings (as in, e.g., North America) and then for 13-channel Wi-Fi 4 (as in, e.g., Europe) (Sections 2.3 and 2.4).

Our results show that, on average, the use of channel bonding in an 11-channel Wi-Fi 4 setting yields a decrease in

performance, although there may be some clusters of STAs reaping significant benefits at the expense of the others, which yields fairness concerns. This essentially matches the premises and conclusions in the consensus about channel bonding so far. However, for the 13-channel setting, our results show a consistent advantage of using channel bonding, contrary to the previous belief. The potential fairness issues remain, which opens interesting avenues for future work as we discuss in Section 4.

2. Wi-Fi 4 Network Model

2.1. Wi-Fi Networks. IEEE 802.11 networks, commercially known as Wi-Fi, are the most widespread technology to deploy wireless local area networks (WLANs). Although Wi-Fi networks can operate in ad hoc and infrastructure modes, in this work we focus on the infrastructure mode, as it is the most widely used. In this operating mode, all the communications occur between access points (APs) and their associated stations (STAs), so if two STAs want to communicate to each other, this communication must go through an AP.

One of the main features of Wi-Fi networks is that this type of networks operates in unlicensed frequency bands. Among these frequency bands, we can highlight the spectrum around 2.4 GHz and the spectrum around 5 GHz. Although the 5 GHz band offers higher bandwidth and throughput, the 2.4 GHz is still the most widely used frequency band due to its better coverage and its compatibility with more legacy equipment. To overcome the limitations in bandwidth, Wi-Fi standards have proposed the use of wider frequency channels, which is called *channel bonding*. More specifically, IEEE 802.11n (Wi-Fi 4) proposes the use of 40 MHz channels instead of the classic 20 MHz ones. Later standards open the possibilities of channel bonding to other bands and wider channel widths, up to 160 MHz. In this paper, we will focus on the Wi-Fi 4 standard in the 2.4 GHz band.

2.2. Graph Modeling. To evaluate the effect of channel bonding in dense Wi-Fi networks, we make use of graph models that accurately represent the peculiarities of this type of networks. In fact, our models represent a set of independent Wi-Fi networks spatially distributed and modeled using geometric graphs. A graph can be defined as a set of vertices V and a set of edges E between them, $E \subseteq \{(u, v) | u, v \in V\}$. In our case, we consider geometric graphs, because the spacial positions of both APs and STAs (which will be the two kinds of vertices in our graphs) have a strong influence in the performance of the network [22]. In our graph model, we will also have two types of edges, one type representing the association between STAs and APs and the other type representing the interfering signals between wireless devices of different networks. To model interferences, we use an activity factor to account for the fact that STAs and APs do not transmit continuously, and we assume higher ψ for APs. Although in this paper we consider 3D graphs, for the sake of an easier visualization, Figure 1 shows

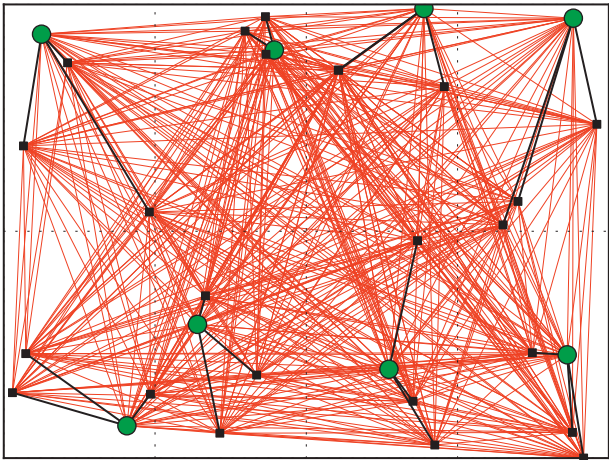


FIGURE 1: Example of Wi-Fi networks modeled with a graph.

a 2D example of the Wi-Fi layout for a single floor of a building, composed of 8 flats, 8 APs (one AP per flat), and 24 STAs (3 STAs per AP). We represent the APs as green circles and the STAs as black squares. Regarding edges, black segments represent the associations between APs and STAs, while red segments represent the interfering signals.

We have made use of a graph-based model for the following reasons. Although we have used discrete event simulators in the context of wireless networks in the past [26], we have noted that those papers that study dense Wi-Fi networks using simulation are difficult to replicate, especially because of the effect of the interferences between adjacent channels [27], which are not negligible at all in dense Wi-Fi settings. For that reason, we chose a graph model that can capture a high number of Wi-Fi network features (not with the precision of simulation models) but is faster and easier to replicate and to use by other researchers for comparison.

2.3. Propagation, Interferences, SINR, and Throughput Computation. Once we have the graph that represents the Wi-Fi layout, we must define how we can compute the achieved throughput for each STA. First of all, it is important to emphasize that the geometry of the problem defines the distances of the different Wi-Fi elements, so with a proper propagation model, we will be able to compute the received signals from the different Wi-Fi elements, being either the desired signal or, mostly, interferences. As we focus on indoor Wi-Fi environments (dense Wi-Fi networks are usually indoor networks), we have used the propagation model defined by the ITU-R in the Recommendation P.1238-10 [28], as it assumes that STAs and APs are in the same building, which will be our testing scenario. Moreover, the ITU-R propagation model also considers losses across different building floors. In [28], propagation losses (in dB) are defined by

$$L_{\text{total}} = 20 \log_{10} f - 28 + N \log_{10} d + L_f(n), \quad (1)$$

with f being the frequency expressed in MHz, N the distance power loss coefficient, d the distance in meters, and $L_f(n)$ the floor penetration factor when signal goes across n

floors. For the 2.4 GHz frequency band, [28] defines $N = 28$ in residential environments, although it is admitted that propagation through walls increases this value considerably. Therefore and according to [29], we have considered $N = 28$ when $d < 16$ meters and $N = 38$ for $d \geq 16$ meters. Finally, according to [28], the losses across two floors when using concrete are 10 dB, so we have considered $L_f(n) = 10n$.

After computing the propagation losses, we can compute the signal power (expressed in dBm) received by an AP or STA i from another Wi-Fi element j as

$$P_r^{j \rightarrow i} = P_t^j + G_j + G_i - L_{\text{total}}, \quad (2)$$

where P_t^j represents the transmission power of j (in dBm) and G_j (or G_i) stands for the transmission (or reception) antenna gain (in dB).

Next, we explain how we compute in the model the interferences received at a device i . In general, a device i will receive interferences from all the transmitting devices in the whole network, excepting from the devices that belong to its same cluster, as their communications are coordinated and do not interfere. Note that a cluster defines the set made by an AP and all its associated STAs. The power of the interfering signal received at device i from device j ($I_r^{j \rightarrow i}$) will be the power of the received signal from j , i.e., $P_r^{j \rightarrow i}$. However, the interference will only be relevant to the device i to the extent that there is an overlap between the spectrum masks (in the frequency domains) as the communications between devices from the same cluster are coordinated and do not interfere. The model accounts for this overlap by means of parameter κ . If both channels are the same, we will consider a total overlap and $\kappa = 1$. On the contrary, if both channels do not collide in the spectrum (orthogonal channels), we will have $\kappa = 0$. Finally, if both channels partially collide, we will consider values of κ ranging from 0 to 1. In addition, we must also consider that, to account for the interference produced from device j to device i , device j is not making use of the spectrum continuously, from a temporal point of view. That behavior is considered by means of the activity factor ψ introduced in Section 2, which can be either ψ_{AP} or ψ_{STA} depending on whether the interfering source is an AP or a STA, respectively. In a sense, factor ψ represents the CSMA/CA (Carrier Sense Multiple Access with Collision Avoidance) behavior of Wi-Fi networks. Some works [30] have modeled it as a Continuous Time Markov Chain (CTMC), concluding that when a STA or AP wants to transmit a packet with probability P_{STA} (or P_{AP} , respectively), it will succeed with probability P_s . For that reason, ψ_{AP} can be computed as $\psi_{AP} = P_{AP} \cdot P_s$, and, equivalently, $\psi_{STA} = P_{STA} \cdot P_s$. As an AP is expected to transmit with a higher probability than STAs, $P_{AP} > P_{STA}$, and therefore $\psi_{AP} > \psi_{STA}$. In summary, we can compute the interference produced by a device j to a device i ($I_r^{j \rightarrow i}$), in a linear scale, by considering the power of the received signal ($P_r^{j \rightarrow i}$), the frequency overlap of their transmission/reception channels (κ), and the activity factor that accounts for the fraction of time during which the interference is being produced (ψ):

$$I^{j \rightarrow i} = P_r^{j \rightarrow i} \cdot \psi \cdot \kappa. \quad (3)$$

From the computation of the desired signal and all the interferences, for a specific STA, it is straightforward to compute the Signal-to-Interference-plus-Noise Ratio (SINR), as it is the quotient of the received power of the signal from its associated AP divided by the sum of the power of all the interfering signals plus the thermal noise. Note that the thermal noise depends on the channel bandwidth, so we consider its value to be -101 dBm for 20 MHz channels and -98 dBm when using channel bonding (with 40 MHz channels).

Finally, to compute the downlink throughput perceived by a STA, we must use the SINR together with the modulation and coding scheme (MCS) used. Depending on the SINR, Wi-Fi 4 [31] defines a specific MCS to be used, which in turn determines the throughput achieved by the STA. As the SINR is higher, it is possible to use modulations with a higher number of bits per symbol and coding schemes with less redundancy. These predefined MCSs, together with the throughput of each MCS for 20 MHz and 40 MHz channels, as defined in the standard [31], are shown in Table 1. Moreover, the table also shows the different SINR thresholds that determine the use of a specific MCS, according to [32].

2.4. Channel Assignment. One of the main configuration challenges in Wi-Fi networks is the choice of the channel to operate in, as defined in Section 1. There have been many works [3,33–35] focused on channel assignment for different Wi-Fi networks. However, channel assignment in uncoordinated Wi-Fi networks is usually based on a local decision based on using the channel where the perceived interference power is minimal [36], so this will be the channel assignment technique considered in this work. More specifically, in the channel selection algorithm, we have considered that each AP periodically scans the spectrum and chooses the channel where it detects the minimum power of interfering signals. This procedure operates asynchronously among the APs changing the order in which the different APs scan the environment. Note that this channel selection procedure represents the usual situation when a user sets up his/her AP leaving the channel selection to a decision of the AP, typically using the option called “Auto” instead of forcing the use of a specific channel. Moreover, as is commonly accepted and as has been suggested in previous works like [22], we restrict the possible channels to be used to the orthogonal channels, so they do not interfere with each other. However, the width of the 2.4 GHz in North America does not allow to use two 40 MHz channels that are totally orthogonal (i.e., nonoverlapping), so we have considered a case where there is some interference between the most separate channels in the spectrum. This will be described in detail in Section 3.3.

3. Performance Evaluation

In this section, we provide an in-depth evaluation of channel bonding in Wi-Fi 4 when operating in the 2.4 GHz frequency band. After a description of the real-world model we have

considered, we perform a validation of the model using the well-known ns-3 simulator [37]. Then, we study channel bonding in two different settings. First, we consider the spectrum that can be used in North America, consisting of 11 channels with 20 MHz width each. For the sake of simplicity, we will name this setting *2.4 GHz USA*. Second, we consider the setting where there are 13 possible channels in the frequency band, as in many parts of the world including Europe. We will name this last setting *2.4 GHz Europe*. Finally, we conduct an analysis of fairness when using channel bonding.

3.1. Experimental Setting. The evaluation of channel bonding has been performed in a three-dimensional realistic setting that represents a five-floor residential building. This scenario is a typical example of a dense uncoordinated Wi-Fi 4 network. The dimensions of the building are $40 \times 30 \times 15$ meters (respectively, length, width, and height; thus, each floor has a height of 3 meters). Each floor has 8 different flats in a 4×2 arrangement. Regarding the distribution of Wi-Fi networks, we consider that each flat has a single AP and a number η of STAs attached to that AP. Note that all the STAs from a flat are attached to the AP from the same flat, which can be the closest AP or not. Moreover, we have considered a wide range of density of STAs in this setting, ranging from $\eta = 1$ STA per AP to $\eta = 12$ STAs per AP. The position of each AP and associated STAs is limited to its flat, with its position in the x - and y -axis being randomly distributed according to a uniform distribution. However, in the z -axis, each AP and each STA is randomly distributed with a normal distribution with a mean of 1.5 meters and a standard deviation of 0.5 meters, bounded to the limits of the floor. To sum up, all the scenarios under study consist of $8 \times 5 = 40$ flats and their corresponding 40 APs and a number of STAs ranging from 40 (when $\eta = 1$) to $12 \times 40 = 480$ (when $\eta = 12$). Finally, for each specific layout, we have considered 5 different settings to account for the randomness in the deployment of the different Wi-Fi elements, for a total of 60 scenarios. Figure 2 shows a graphical representation of two of the scenarios under study, where, for the sake of clarity, we only show the association between APs and STAs.

Finally, Table 2 defines the values used for the main parameters needed to compute the throughput, which in all cases are typical or reasonable values.

3.2. Model Validation. For validation purposes, in this section we include a comparative evaluation of the results obtained using our proposed model with respect to the equivalent results obtained using a discrete event simulator. More specifically, we have chosen the well-known ns-3 simulator [37]. The reference setting for this validation consists of a single AP and a single STA (attached to that AP) positioned at different distances. As our model computes the highest reachable throughput that a STA is able to obtain, in the simulator we have considered a greedy traffic source that emits UDP datagrams with a rate higher than the maximum throughput that the technology permits. To make the results

TABLE 1: Relation between MCS, SINR, and throughput in Wi-Fi 4 with mandatory 800 ns guard interval (GI) [31].

MCS index	Modulation scheme	Coding rate	Throughput for 20 MHz (Mbit/s)	Throughput for 40 MHz (Mbit/s)	SINR range (dB) [32]
0	BPSK	1/2	6.5	13.5	[6.8, 7.9)
1	QPSK	1/2	13.0	27.0	[7.9, 10.6)
2	QPSK	3/4	19.5	40.5	[10.6, 13.0)
3	16-QAM	1/2	26.0	54.0	[13.0, 17.0)
4	16-QAM	3/4	39.0	81.0	[17.0, 21.8)
5	64-QAM	2/3	52.0	108.0	[21.8, 24.7)
6	64-QAM	3/4	58.5	121.5	[24.7, 28.1)
7	64-QAM	5/6	65.0	135.0	> 28.1

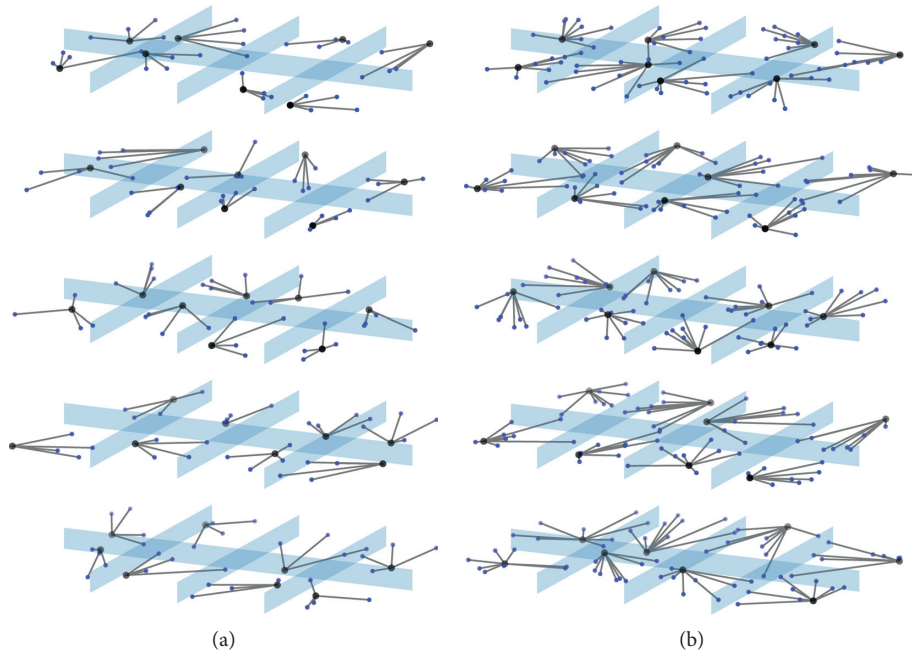


FIGURE 2: Examples of scenarios. (a) $\eta = 4$. (b) $\eta = 8$.

TABLE 2: Summary of parameters.

Parameter	Value
P_t	30 mW
G_t	0 dB
G_r	0 dB
Ψ_{AP}	0.5
Ψ_{STA}	0.1

comparable, we have used in ns-3 the same indoor propagation model, i.e., ITU-R P.1238-10, and we have configured the Wi-Fi manager in the simulator according to the settings used in our experiments.

The validation of our model has been conducted in a two-step procedure. First, at the physical level, we compare the received SINR, as is shown in Figure 3. We can see that both curves totally coincide, validating that our model and the ns-3 simulator obtain the same SINR. As a second step, we study the throughput obtained by the STA with our model and the simulator, as is shown in Figure 4. In that figure, we notice that the shapes of the curves coincide in both cases. However, there is a clear offset between both

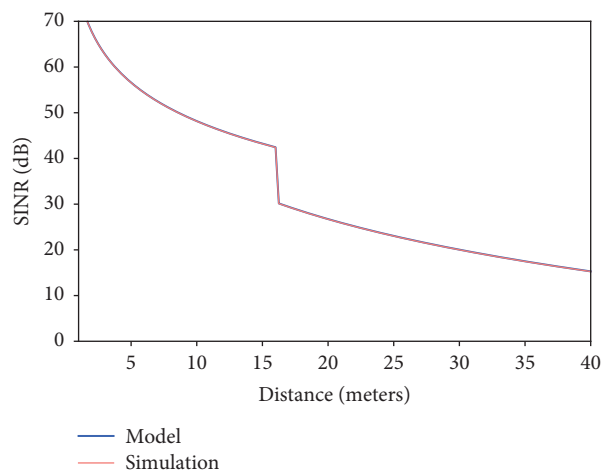


FIGURE 3: SINR obtained by our proposed model and by the ns-3 simulator.

curves. This behavior is due to the fact that our model measures the physical throughput, while ns-3 computes the throughput at the application layer (usually called goodput),

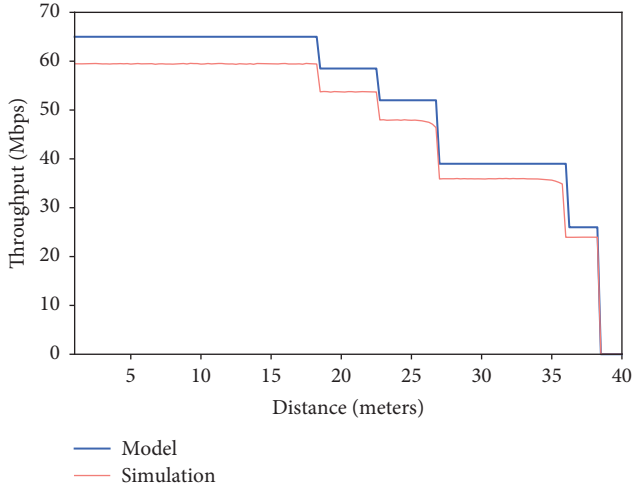


FIGURE 4: Throughput obtained by our proposed model and by the ns-3 simulator. *Note.* The model gives throughput at the physical layer, while the simulator measures goodput (application layer throughput).

with the difference between both values being the overhead introduced by the different layers of the protocol stack. That is the reason of measuring a higher throughput in our model, although both throughput measures coincide.

3.3. Channel Bonding in the 2.4 GHz USA Frequency Band.

In this section, we evaluate the effect that channel bonding has on the throughput perceived by users when they operate in the 2.4 GHz frequency band with 11 nonorthogonal channels, which is the situation occurring in North America. In this setting, when using 20 MHz channels, there are three different orthogonal channels, being channels 1, 6, and 11. However, since the spectrum band goes from 2401 MHz to 2473 MHz, we cannot use two different 40 MHz orthogonal channels. Therefore, by placing one 40 MHz channel in the lowest part of the spectrum and another 40 MHz channel in the highest part, both channels will collide in the frequency band between 2433 and 2441 MHz. For that reason, we have considered that the interference index (κ) when using two 40 MHz channels in the 2.4 GHz USA frequency band is $(2441 - 2433)/40 = 0.2$. In other words, both channels, as they cannot be orthogonal, collide with a factor of $\kappa = 0.2$, producing interferences to each other. Finally, for the sake of completeness, we have also considered the situation where we only use one 40 MHz channel in the 2.4 GHz USA frequency band, since this is the only possibility for totally orthogonal channels in this setting. Figure 5 shows the average downlink throughput and 95% confidence intervals that users can achieve when we consider either three orthogonal 20 MHz channels, two (nonorthogonal) 40 MHz channels, or one orthogonal 40 MHz channel. For each value of η , the average throughput has been computed averaging the five different deployments that we have considered for each value of η and running 10 executions for each of those five deployments. The rationale for performing 10 runs for each setting is that channel assignment technique used (as described in Section 3.4) is not deterministic (except when we make use of a unique 40 MHz

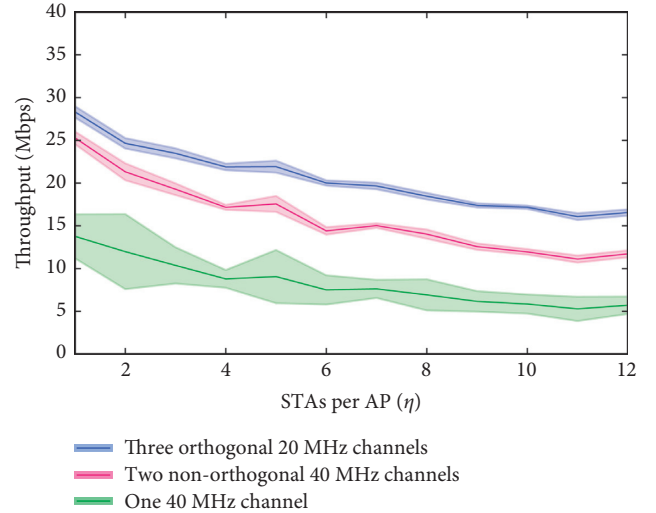


FIGURE 5: Comparison of average throughput in the 2.4 GHz USA frequency band.

channel). As it could be expected, the achieved throughput decreases as the density of STAs (η) increases. Moreover, results show that, on average, in the 2.4 GHz USA frequency band, it is not recommended that channel bonding is used, as the gain that can be obtained by using channels with a higher bandwidth has a lower effect than that of having a fewer number of orthogonal channels, even when the density of users is low ($\eta = 1$). Additionally, we can also conclude that it would be better to use two 40 MHz channels (although they are not completely orthogonal) than to use only one 40 MHz channel.

Now, we perform a more in-depth analysis of the throughput that STAs can achieve individually. In Table 3 we show, for the different densities of STAs (η) under consideration, the percentage of STAs that increase (+), keep the same (=), or decrease (-) their downlink throughput when using channel bonding with two nonorthogonal 40 MHz channels, compared to the situation where three orthogonal 20 MHz channels are used. Moreover, the table also shows the average increase (or decrease) in throughput for the STAs that get better (or worse) performance when using channel bonding with two 40 MHz channels. Inspecting Table 3, we observe that the percentage of STAs that improve their throughput is lower than the percentage of STAs that get a worse throughput, even with the lowest density of STAs, where only 26.5% of STAs fare better in terms of bandwidth and 65% fare worse. This confirms the common belief that, in dense scenarios, it is not recommended that channel bonding is used in the 2.4 GHz USA frequency band. In addition, Table 3 shows that, even when the majority of STAs get a worse throughput, the average gain for the “improving” STAs is higher than the loss for the “losing” STAs, which can create fairness issues and misalignment of incentives in network management for these settings. Since the use of channel bonding is local to APs, the managers of some of the networks could unilaterally decide to transmit in 40 MHz channels at the expense of the networks nearby. Even for those networks which, on average, “lose” throughput by using channel bonding, the fact that when the

TABLE 3: Percentage of STAs that increase (+)/keep (=)/decrease (–) their throughput (and average increase/decrease) using channel bonding with two nonorthogonal 40 MHz channels in the 2.4 GHz USA setting.

η	% STA			Increase/decrease (Mbps)	
	+	=	–	Increase	Decrease
1	26.50	8.50	65.00	20.29	–13.27
2	23.75	7.75	68.50	20.42	–12.49
3	21.83	9.50	68.67	19.00	–12.36
4	18.38	9.25	72.38	19.79	–11.84
5	17.90	11.10	71.00	20.02	–11.56
6	15.83	13.08	71.08	17.59	–11.90
7	16.29	14.36	69.36	17.70	–11.08
8	14.75	13.88	71.38	17.51	–10.45
9	13.56	15.83	70.61	17.31	–10.89
10	12.95	17.40	69.65	17.66	–10.89
11	12.64	18.45	68.91	15.95	–11.05
12	12.67	18.88	68.46	17.15	–10.48

load in the neighboring networks is low, the effective throughput is higher (because of using more bandwidth) may make managers choose to use channel bonding, thus hampering average performance for the network.

We now perform a similar analysis for the comparison of the gain of using one 40 MHz channel with respect to using three 20 MHz orthogonal channels (Table 4). As expected, the use of only one 40 MHz channel is not recommendable, and the number of users that can improve their throughput is very low, ranging from 8% ($\eta = 1$) to 2.73% ($\eta = 10$). We see again that the average throughput increase for “winning” STAs is higher than the decrease for “losing” STAs, but this difference is not as remarkable as in the case of two non-orthogonal 40 MHz channels.

Finally, Figures 6 and 7 show a ridge plot to evaluate the difference in the throughput that each STA can obtain when using two nonorthogonal 40 MHz channels instead of three orthogonal 20 MHz channels (Figure 6) or one 40 MHz channel instead of three orthogonal 20 MHz channels (Figure 7). Note that both figures represent the probability density functions expressed as a Kernel Density Estimation (KDE). In both figures, we observe that the number of STAs that decrease their throughput when using channel bonding (the area to the left of the vertical line at 0) is higher than the number of STAs that improve their throughput (the area to the right). Moreover, the tail on the right side of each KDE is longer than the tail on the left side, reflecting that there are STAs which greatly increase their throughput with channel bonding. Finally, inspecting the figures as the density of the Wi-Fi scenarios increases (i.e., moving vertically from bottom to top), we conclude that channel bonding in the 2.4 GHz USA frequency band is even a worse choice when the density of the Wi-Fi network increases.

3.4. Channel Bonding in the 2.4 GHz Europe Frequency Band.

In this section, we perform a similar evaluation to the one provided in the previous section, but now focusing on the 2.4 GHz frequency band where there are at least thirteen

TABLE 4: Percentage of STAs that increase (+)/keep (=)/decrease (–) their throughput (and average increase/decrease) using channel bonding with one 40 MHz channel in the 2.4 GHz USA setting.

η	% STA			Increase/decrease (Mbps)	
	+	=	–	Increase	Decrease
1	8.00	8.50	83.50	23.38	–19.57
2	7.25	7.75	85.00	24.07	–17.13
3	6.17	9.50	84.33	22.51	–17.27
4	5.13	9.25	85.63	21.63	–17.11
5	4.70	11.10	84.20	22.60	–16.89
6	4.33	13.00	82.67	17.40	–16.23
7	4.00	14.21	81.79	20.47	–16.06
8	3.31	13.81	82.88	19.12	–15.15
9	3.17	15.78	81.06	19.46	–15.26
10	2.70	17.30	80.00	20.46	–15.07
11	2.73	18.36	78.91	14.88	–14.98
12	2.83	18.88	78.29	16.74	–14.81

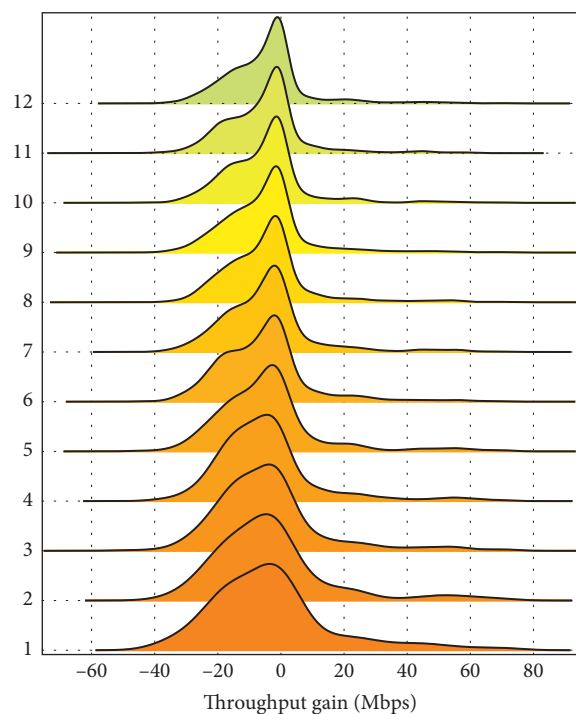


FIGURE 6: Density of the throughput gain of using channel bonding with two 40 MHz channels in the 2.4 GHz USA setting.

20 MHz channels available, as in most of the world and in particular in Europe. In this case, it is possible to use two 40 MHz orthogonal channels, so we will compare two situations: using two orthogonal 40 MHz channels and using three orthogonal 20 MHz channels. Figure 8 shows the average downstream throughput achieved by STAs in both situations. As opposed to the behavior of the 2.4 GHz USA frequency band, in this 2.4 GHz Europe frequency band, the average throughput achieved increases when using channel bonding. Although the advantage of using channel bonding diminishes with the density of STAs (η), it is always advantageous even in the more dense scenarios.

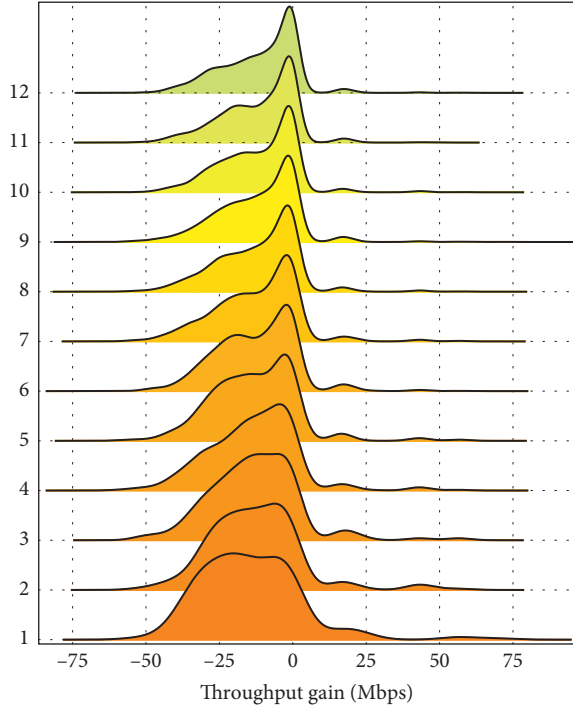


FIGURE 7: Density of the throughput gain of using channel bonding with one 40 MHz channel in the 2.4 GHz USA setting.

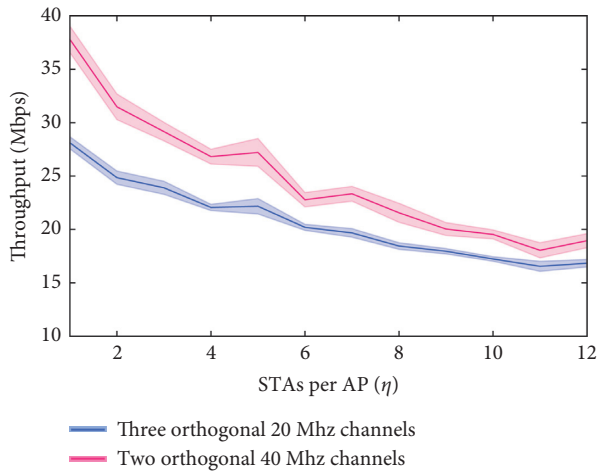


FIGURE 8: Comparison of average throughput in the 2.4 GHz Europe frequency band.

Table 5 shows the number of STAs that are able to increase their throughput when using channel bonding. In general, for the lowest values of η , the percentage of STAs that increase their throughput is higher than the percentage of STAs that decrease it, but this is not true when the density of STAs increases. Furthermore, the average throughput gain of those STAs that improve their throughput is remarkably higher (around 19 to 23 Mbps) than the decrease of those STAs that get a worse throughput (around 6.5 to 9 Mbps).

Finally, in Figure 9, we show the KDE of the difference in the throughput perceived by STAs when using channel bonding, where we can remark the longer tails on the right of

TABLE 5: Percentage of STAs that increase (+)/keep (=)/decrease (-) their throughput (and average increase/decrease) with two orthogonal 40 MHz channels in the 2.4 GHz Europe setting.

η	% STA			Increase/decrease (Mbps)	
	+	=	-	Increase	Decrease
1	55.00	8.50	36.50	23.52	-9.03
2	45.75	7.75	46.50	22.42	-8.20
3	44.33	9.33	46.33	20.48	-7.33
4	41.38	9.25	49.38	20.25	-7.24
5	41.30	11.10	47.60	19.77	-6.72
6	34.33	13.08	52.58	20.68	-7.05
7	35.36	14.21	50.43	19.93	-6.59
8	32.31	13.94	53.75	20.31	-6.10
9	32.11	15.72	52.17	18.99	-6.56
10	28.50	17.40	54.10	19.50	-6.38
11	31.14	18.23	50.64	18.39	-6.66
12	28.96	18.88	52.17	19.03	-6.48

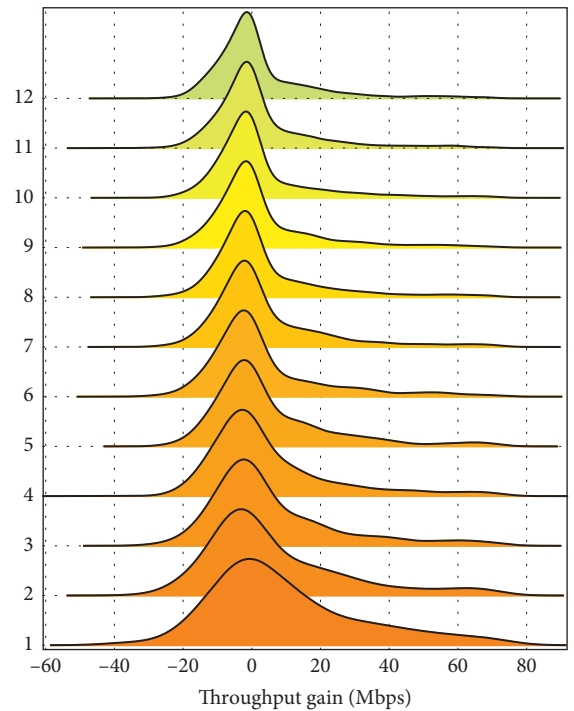


FIGURE 9: Density of the throughput gain of using channel bonding with two orthogonal 40 MHz channels in the 2.4 GHz Europe setting.

the different curves, which shows that the gain of using channel bonding for the “winning” STAs is higher than the loss in throughput for the “losing” ones. Taking this into account, we can conclude that, even when there are a nonnegligible number of STAs that decrease their throughput when using channel bonding, the high increase in an important fraction of STAs makes channel bonding in the 2.4 GHz Europe frequency band worth using.

3.5. *Study of Fairness.* After the study of the throughput and the incentives that STAs can obtain by using channel

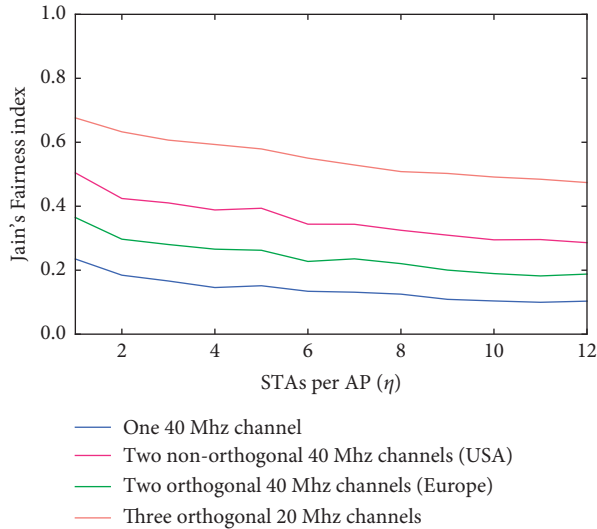


FIGURE 10: Study of fairness.

bonding in different regions, we complete the analysis of channel bonding by studying the fairness of the perceived throughput of the different STAs. The focus is to determine if channel bonding has an effect on fairness. The performance parameter used to measure fairness is the well-known Jain's fairness index [38], defined by

$$f(x) = \frac{[\sum_{i=1}^n Th_i]^2}{\sum_{i=1}^n Th_i^2}, \quad Th_i \geq 0, \quad (4)$$

with Th_i being the downlink throughput perceived by STA i . Jain's fairness index is able to measure the "quality" of the service experienced by the different STAs. If all STAs obtain the same throughput, the fairness index is equal to 1. As the disparity increases, the fairness index goes down to 0, when the system clearly favors selected few users over the rest.

In Figure 10, we show the fairness for the different settings under study. Note that each value of a curve is the average value of the 5 different settings and 10 different executions. Results show that the best fairness is obtained when using three orthogonal 20 MHz channels. This result is due to the fact that the range in throughput is higher when using channel bonding than when not using it. In other words, STAs using channel bonding can obtain a throughput from 0 to 135 Mbps, while the upper value decreases to 65 Mbps when channel bonding is not in use. For this reason, the disparities between STAs when using channel bonding can be higher. The fairness obtained when using two 40 MHz channels is higher in the USA setting than in the Europe setting. Therefore, we can conclude that the advantage in throughput that can be obtained when using two 40 MHz channels in the 2.4 GHz Europe frequency band is at the expense of increasing the disparity between the throughputs obtained by the different STAs.

4. Conclusions

Channel bonding is a technique proposed in Wi-Fi networks since the standard IEEE 802.11n (Wi-Fi 4) to use wider frequency channels to be able to obtain higher throughputs.

However, its use is usually discouraged in the 2.4 GHz frequency band, since it only allows for two 40 MHz orthogonal (or almost orthogonal) channels. However, we found a number of limitations in previous studies on the matter, so we revised that belief for dense, uncoordinated Wi-Fi 4 environments. Our study confirms the previous consensus that it is not advisable to use channel bonding in the 2.4 GHz frequency band with 11 channels which are 20 MHz wide (as in North America). However, contrary to the usual assumption, we show that the use of channel bonding with 40 MHz channels in the 2.4 GHz frequency band with 13 or more 20 MHz channels (the one used in many parts of the world, including Europe) results in an improvement of the average throughput achieved by STAs. Moreover, we show that, even when the number of STAs that decrease their throughput is not negligible, the improvement in throughput experienced by the "winning" STAs is much higher than the decrease in throughput experienced by the "losing" STAs. Hence, channel bonding is worth using not only from the perspective of getting a higher sum of throughputs for the network, but also from the perspective of STAs.

As the decision of using channel bonding lies in the AP but the benefits are for STAs, as a future work, we plan to shift to the STAs (therefore to the users) the decision of whether to use channel bonding or not, since these are ultimately the ones impacted by such decisions. Such a possibility will let us reach more democratic, client-centric configurations, with which we intend to address the fairness issues usually related to channel bonding. Finally, we want to explore the effects of dynamic channel bonding in the 2.4 GHz band, since it could significantly increase the advantage of using channel bonding techniques in Wi-Fi 4.

Data Availability

The graphs used to support the findings of this study are available from the corresponding author upon request.

Conflicts of Interest

The authors declare that they have no conflicts of interest.

Acknowledgments

Jose Manuel Gimenez-Guzman, Ivan Marsa-Maestre, David Orden, and Susel Fernandez were partially funded by Project SBPLY/19/180 501/000 171 of the Junta de Comunidades de Castilla-La Mancha and FEDER and by Project UCeNet (CM/JIN/2019-031) of the Comunidad de Madrid and University of Alcalá. Jose Manuel Gimenez-Guzman, Ivan Marsa-Maestre, and Susel Fernandez were also funded by Project PID2019-104855RB-I00/AEI/10.130 39/501 100 011 033 of the Spanish Ministry of Science and Innovation. David Orden was also partially supported by Project PID2019-104129GB-I00/AEI/10.130 39/501 100 011 033 of the Spanish Ministry of Science and Innovation and by H2020-MSCA-RISE Project 734 922 - CONNECT. Marino Tejedor-Romero was funded by a predoctoral contract from University of Alcalá.

References

- [1] V. Sathya, M. I. Rochman, and M. Ghosh, "Measurement-based coexistence studies of LAA & wi-fi deployments in chicago," *IEEE Wireless Communications*, vol. 28, no. 1, pp. 136–143, 2021.
- [2] H. A. Omar, K. Abboud, N. Cheng, K. R. Malekshan, A. T. Gamage, and W. Zhuang, "A survey on high efficiency wireless local area networks: next generation wifi," *IEEE Communications Surveys & Tutorials*, vol. 18, no. 4, pp. 2315–2344, 2016.
- [3] S. Chiochan, E. Hossain, and J. Diamond, "Channel assignment schemes for infrastructure-based 802.11 WLANs: a survey," *IEEE Communications Surveys & Tutorials*, vol. 12, no. 1, 2010.
- [4] E. de la Hoz, J. Gimenez-Guzman, I. Marsa-Maestre, and D. Orden, "Automated negotiation for resource assignment in wireless surveillance sensor networks," *Sensors*, vol. 15, no. 11, pp. 29547–29568, 2015.
- [5] H.-J. Chen, C.-P. Chuang, Y.-S. Wang, S.-W. Ting, H.-Y. Tu, and C.-C. Teng, "Design and implementation of a cluster-based channel assignment in high density 802.11 WLANs," in *Proceedings of the Network Operations and Management Symposium (APNOMS), 2016 18th Asia-Pacific*, pp. 1–5, IEEE, Kanazawa, Japan, October 2016.
- [6] Y. M. Kwon, K. Choi, M. Kim, and M. Y. Chung, "Distributed channel selection scheme based on the number of interfering stations in WLAN," *Ad Hoc Networks*, vol. 39, pp. 45–55, 2016.
- [7] H. Kasasbeh, F. Wang, L. Cao, and R. Viswanathan, "Generous throughput oriented channel assignment for infrastructure WiFi networks," in *Proceedings of the Wireless Communications and Networking Conference (WCNC)*, pp. 1–6, IEEE, San Francisco, CA, USA, March 2017.
- [8] D. Orden, I. Marsa-Maestre, J. M. Gimenez-Guzman, E. de la Hoz, and A. Álvarez-Suárez, "Spectrum graph coloring to improve Wi-Fi channel assignment in a real-world scenario via edge contraction," *Discrete Applied Mathematics*, vol. 263, pp. 234–243, 2019.
- [9] S. H. R. Bukhari, M. H. Rehmani, and S. Siraj, "A survey of channel bonding for wireless networks and guidelines of channel bonding for futuristic cognitive radio sensor networks," *IEEE Communications Surveys & Tutorials*, vol. 18, no. 2, pp. 924–948, 2015.
- [10] S. Barrachina-Muñoz, F. Wilhelmi, and B. Bellalta, "To overlap or not to overlap: enabling channel bonding in high-density w lans," *Computer Networks*, vol. 152, pp. 40–53, 2019.
- [11] L. Lanante and S. Roy, "Analysis and optimization of channel bonding in dense ieee 802.11 w lans," *IEEE Transactions on Wireless Communications*, vol. 20, no. 3, pp. 2150–2160, 2021.
- [12] L. Deek, E. Garcia-Villegas, E. Belding, S.-J. Lee, and K. Almeroth, "The impact of channel bonding on 802.11 N network management," in *Proceedings of the Seventh Conference on Emerging Networking Experiments and Technologies*, pp. 1–12, Tokyo, Japan, December 2011.
- [13] S.-H. Lim, Y.-B. Ko, C. Kim, and N. H. Vaidya, "Design and implementation of multicasting for multi-channel multi-interface wireless mesh networks," *Wireless Networks*, vol. 17, no. 4, pp. 955–972, 2011.
- [14] L. Deek, E. Garcia-Villegas, E. Belding, S.-J. Lee, and K. Almeroth, "Joint rate and channel width adaptation for 802.11 mimo wireless networks," in *Proceedings of the 2013 IEEE International Conference on Sensing, Communications and Networking (SECON)*, pp. 167–175, IEEE, New Orleans, LA, USA, October 2013.
- [15] J. Fang and I. T. Lu, "Efficient channel access scheme for multiuser parallel transmission under channel bonding in IEEE 802.11ac," *IET Communications*, vol. 9, no. 13, pp. 1591–1597, 2015.
- [16] Y. Daldoul, D.-E. Meddour, and A. Ksentini, "IEEE 802.11 ac: effect of channel bonding on spectrum utilization in dense environments," in *Proceedings of the 2017 IEEE International Conference on Communications (ICC)*, pp. 1–6, IEEE, Paris, France, May 2017.
- [17] S. Barrachina-Muñoz, F. Wilhelmi, and B. Bellalta, "Dynamic channel bonding in spatially distributed high-density w lans," *IEEE Transactions on Mobile Computing*, vol. 19, no. 4, pp. 821–835, 2019.
- [18] Z. Khan, H. Ahmadi, E. Hossain, M. Coupechoux, L. A. Dasilva, and J. J. Lehtomäki, "Carrier aggregation/channel bonding in next generation cellular networks: methods and challenges," *IEEE Network*, vol. 28, no. 6, pp. 34–40, 2014.
- [19] D. A. Marendra, G. M. Suranegara, S. Qamar, R. Hakimi, and E. Mulyana, "Emulating software-defined wireless network: bicasting scenario," in *Proceedings of the 2017 3rd International Conference on Wireless and Telematics (ICWT)*, pp. 76–80, Palembang, Indonesia, July 2017.
- [20] CISCO, *802.11ac: The Fifth Generation of Wi-Fi, Cisco System Technical White Paper*, CISCO, San Jose, CA, USA, 2018.
- [21] L. Xu, K. Yamamoto, and S. Yoshida, "Performance comparison between channel-bonding and multi-channel csma," in *Proceedings of the 2007 IEEE Wireless Communications and Networking Conference*, pp. 406–410, Hong Kong, China, March 2007.
- [22] J. M. Gimenez-Guzman, I. Marsa-Maestre, D. Orden, E. de la Hoz, and T. Ito, "On the goodness of using orthogonal channels in WLAN IEEE 802.11 in Realistic Scenarios," *Wireless Communications and Mobile Computing*, vol. 2018, Article ID 5742712, 11 pages, 2018.
- [23] Texas Instruments, *Wlan Channel Bonding: Causing Greater Problems than it Solves*, Texas Instruments, Dallas, Texas, USA, 2003.
- [24] R. Chandra, R. Mahajan, T. Moscibroda, R. Raghavendra, and P. Bahl, "A case for adapting channel width in wireless networks," *ACM SIGCOMM Computer Communication Review*, vol. 38, no. 4, pp. 135–146, 2008.
- [25] V. Shrivastava, S. Rayanchu, J. Yoonj, and S. Banerjee, "11 n under the microscope," in *Proceedings of the 8th ACM SIGCOMM Conference on Internet Measurement*, pp. 105–110, Greece, 2008.
- [26] J. Martinez-Bauset, J. Gimenez-Guzman, and V. Pla, "Optimal admission control in multimedia mobile networks with handover prediction," *IEEE Wireless Communications*, vol. 15, no. 5, pp. 38–44, 2008.
- [27] A. M. Voicu, L. Lava, L. Simić, and M. Petrova, "The importance of adjacent channel interference: experimental validation of ns-3 for dense wi-fi networks," in *Proceedings of the 20th ACM International Conference on Modelling, Analysis and Simulation of Wireless and Mobile Systems*, pp. 43–52, Miami, FL, USA, November 2017.
- [28] Rec ITU-R P 1238-8, *Propagation Data and Prediction Methods for the Planning of Indoor Radiocommunication Systems and Radio Local Area Networks in the Frequency Range 300 MHz to 100 GHz*, International Telecommunication Union, Geneva, Switzerland, 2015.
- [29] T. Chrysikos, G. Georgopoulos, and S. Kotsopoulos, "Site-specific validation of itu indoor path loss model at 2.4 GHz," in *Proceedings of the 2009 IEEE International Symposium on*

- World of Wireless, Mobile and Multimedia Networks & Workshops*, pp. 1–6, IEEE, Kos, Greece, 2009.
- [30] Mukta and N. Gupta, “Analytical approach towards available bandwidth estimation in wireless Ad Hoc networks,” *Wireless Networks*, vol. 26, no. 10, pp. 1–26, 2020.
- [31] IEEE Computer Society, “IEEE standard for information technology– local and metropolitan area networks– Specific requirements– Part 11: Wireless LAN Medium Access Control (MAC) and Physical Layer (PHY) specifications amendment 5: enhancements for higher throughput,” in *Proceedings of the IEEE Std 802.11n-2009 (Amendment To IEEE Std 802.11-2007 as Amended by IEEE Std 802.11k-2008, IEEE Std 802.11r-2008, IEEE Std 802.11y-2008, and IEEE Std 802.11w-2009)*, pp. 1–565, 2009.
- [32] M. Kim and C.-H. Choi, “Hidden-node detection in IEEE 802.11n wireless LANs,” *IEEE Transactions on Vehicular Technology*, vol. 62, no. 6, pp. 2724–2734, 2013.
- [33] E. De La Hoz, I. Marsa-Maestre, J. M. Gimenez-Guzman, D. Orden, and M. Klein, “Multi-agent nonlinear negotiation for Wi-Fi channel assignment,” in *Proceedings of the 16th Conference on Autonomous Agents and MultiAgent Systems*, pp. 1035–1043, Sao Paulo, Brazil, 2017.
- [34] C. Camacho-Gómez, I. Marsa-Maestre, J. M. Gimenez-Guzman, and S. Salcedo-Sanz, “A coral reefs optimization algorithm with substrate layer for robust wi-fi channel assignment,” *Soft Computing*, vol. 23, no. 23, pp. 12621–12640, 2019.
- [35] I. Marsa-Maestre, E. de la Hoz, J. M. Gimenez-Guzman, D. Orden, and M. Klein, “Nonlinear negotiation approaches for complex-network optimization: a study inspired by wi-fi channel assignment,” *Group Decision and Negotiation*, vol. 28, no. 1, pp. 175–196, 2019.
- [36] M. Achanta, “Method and apparatus for least congested channel scan for wireless access points,” US Patent App, 2006.
- [37] G. F. Riley and T. R. Henderson, “The Ns-3 Network Simulator,” in *Modeling and Tools for Network Simulation*, pp. 15–34, Springer, Berlin, Germany, 2010.
- [38] R. K. Jain, D.-M. W. Chiu, and W. R. Hawe, “A quantitative measure of fairness and discrimination,” Eastern Research Laboratory, Digital Equipment Corporation, Hudson, MA, USA, 1984.

Review Article

Signal Propagation Models in Soil Medium for the Study of Wireless Underground Sensor Networks: A Review of Current Trends

Frank Kataka Banaseka ^{1,2}, Ferdinand Katsriku,² Jamal Deen Abdulai,² Kofi Sarpong Adu-Manu ² and Felicia Nana Ama Engmann ²

¹Department of Information Technology, University of Professional Studies, Accra, Ghana

²Department of Computer Science, University of Ghana, Legon, Ghana

Correspondence should be addressed to Frank Kataka Banaseka; frank.banaseka@upsamail.edu.gh

Received 10 September 2020; Revised 6 March 2021; Accepted 10 March 2021; Published 5 April 2021

Academic Editor: Ivan Marsa-Maestre

Copyright © 2021 Frank Kataka Banaseka et al. This is an open access article distributed under the Creative Commons Attribution License, which permits unrestricted use, distribution, and reproduction in any medium, provided the original work is properly cited.

Radio signal propagation modeling plays an important role in the design of wireless communication systems. Various models have been developed, over the past few decades, to predict signal propagation and behavior for wireless communication systems in different operating environments. Recently, there has been an interest in the deployment of wireless sensors in soil. To fully exploit the capabilities of sensor networks deployed in soil requires an understanding of the propagation characteristics within this environment. This paper reviews the cutting-edge developments of signal propagation in the subterranean environment. The most important modeling techniques for modeling include electromagnetic waves, propagation loss, magnetic induction, and acoustic wave. These are discussed vis-a-vis modeling complexity and key parameters of the environment including electric and magnetic properties of soil. An equation to model propagation in the soil is derived from the free space model. Results are presented to show propagation losses and at different frequencies and volumetric water content. The channel capacity and the operating frequency are also analyzed against soil moisture at different soil types and antenna sizes.

1. Introduction

Wireless sensor networks are increasingly being used in new applications such as soil and underwater. Such networks are also being used in open underground tunnels and mines mainly to facilitate communication in transport systems and also for safety requirements in mines [1]. This calls for the use of innovative communication techniques in their realization. The wireless underground sensor network (WUSN) is thus one of such emergent areas that have gained the attention of many researchers [2–7]. WUSNs can be defined as a network of wireless devices operating in a subterranean environment. The devices may either be buried at a particular depth in soil or be positioned within an enclosed open underground space such as underground mines and tunnels [2]. The use of WUSNs opens up new possibilities for underground monitoring and communication. Capabili-

ties of WUSNs that make them attractive for use include timely data collection, concealment, easy deployment in hazardous areas, reliability, and coverage of large geographic areas. Research in the area of WUSNs in the past has focused on the deployment of networks in open subterranean environments such as coal mines, subways, or sewer systems [8]. Even though such networks are set up underground, the medium through which communication takes place is still air. The channel characteristics for underground sensor networks and terrestrial sensor networks do however reveal a lot of similarities. The terrestrial WSNs are assumed to operate in unbounded free space whilst WUSNs on the other hand operate in the air but are bounded or confined by soil.

An emerging area of WUSNs is one in which sensor nodes are completely buried in soil and communication takes place within the soil medium (WUSN-BS). These WUSN-BSs have several applications, including monitoring of soil

physical properties for precision agriculture and sports [3]. Additionally, WUSN-BS can be used to detect soil contamination in mining areas or refuse dumpsites. Furthermore, WUSN-BS has military and security applications including intrusion detection, detection of troupe movement, and border patrol.

In this paper, the latest development in signal propagation modeling related to the soil is reviewed. The most important modeling techniques used for propagation in the soil are described. Channel performance measures such as path loss and channel capacity as well as some research challenges are also discussed. They are discussed in terms of modeling complexity and required information on the environment including properties of soil.

2. Related Work

Earlier work has shown that EM techniques for modeling signal propagation may still apply to soil environments [2, 3, 6, 9, 10]. To the best of our knowledge, there is little research work on the channel characterization of EM waves in this environment. The magnetic induction (MI) method is another transmission technique that has been used for short-range communication in soil. As far as underground mines and tunnels are concerned, the use of EM waves has proven to be the most appropriate choice for the characterization of wireless signal propagation, since the medium is still air [2].

The literature on propagation in soil has been growing an indication of the increased interest in the area. It has been suggested that wireless communication through soil may be modeled as EM wave transfer through a transmission line [11]. In [12], the electromagnetic field principles of a dipole in a conducting half-space are analyzed over the frequency range from 1 to 10 MHz. In [13], the principles of the surface-penetrating radar are reviewed and an overview of the empirical attenuation and relative permittivity values of various materials, including soil, at 100 MHz is also presented. In another study, it was shown that the soil composition has significant effects on the ground-penetrating radar (GPR) detection of landmines [14]. A project on glacier monitoring using a network of buried sensors in Norway is presented in [8]. The sensor network in this project is intended to measure the parameters of ice caps and glaciers using sensors beneath the glaciers. The base stations are connected to two wired transceivers 30 m below the surface to avoid wet ice. Using very high transmit powers, communication takes place between the underice sensors and the base stations aboveground. It is observed that part of the signal travels through the glacier and part through the air. To guarantee the safety of mine workers, wireless sensor networks are increasingly being used to monitor underground mines. In this case, the signal propagation takes place in an open bounded area [1, 7, 15, 16]. In another project where a sensor network is used in a sewer system, a manhole cover is converted into a slot antenna. This established communication between sensors underground and the aboveground nodes through radiation from the manhole cover [17]. Once again, although the system is set up underground, the com-

munication is performed through the air. In similar works [10], the characteristics of the wireless channel in tunnels are investigated. In another related work [18], the largest residential water management project in Europe is described. The project deployed a sensor network used to gather information for inspection and cleaning systems in a sewer system.

WUSN was also used for increasing the efficiency of oil recovery processes. In this case, millimeter-scale sensors and antennas are deployed within confined oil reservoir fractures, which necessitates the sensor nodes operating in the terahertz range [19].

In [20], WUSNs have been used to characterize radio transmission between underground buried pipes and a base station using multilayer media. This is to identify the range of operating communication frequencies having lower energy loss, lower bit error rate, and power needed to transfer packets that carry data through the media.

In a more recent study, the complex refractive index model-Fresnel (CRIM-Fresnel) and the modified Fruis are considered the two electromagnetic signal attenuation models used to evaluate the signal strength in soil medium. These models were reviewed, and a methodology was developed to perform an experimental measurement of electromagnetic signal attenuation in the laboratory. Measured results from the laboratory are compared with the estimated values computed from the propagation loss models. A significant difference between the models and estimated values is established from the comparison [21].

In agriculture, IoUT is envisaged to provide total field autonomy and enable more efficient food production solutions through not only in situ monitoring and self-reporting capabilities (soil moisture, salinity, temperature, etc.) but also the interconnection of existing field machinery like irrigation systems, harvesters, and seeders [22, 23]. Enabling communication technologies for the Internet of underground things (IoUT), network issues, and localization techniques are presented in [24]. These enabling technologies include EM wave transmission, MI systems, acoustic wave transmission, wired networks, visible light communication (VLC), and mud pulse telemetry (MPT) communication systems for oil and gas monitoring.

To prolong the lives of energy-hungry sensor nodes in wireless sensor networks, energy management schemes have been proposed in the literature to keep the sensor nodes alive. This is to make the network operational and efficient. These energy management schemes include energy harvesting, energy transfer, and energy conservation [25, 26].

In [27], a new wave number model is proposed using the combination of the Peplinski principle and multiple scattering in soil medium. The new wave number is used in the computation of the path loss. The path loss is modeled based on the absorption due to permittivity and multiple scattering from obstacles in soil. The path loss is then analyzed against distance at two typical IoT frequencies of 433 MHz and 868 MHz. This work also showed the effect of VWC on the path loss for two proportions, 5% and 50%.

Table 1 presents a summary of the contributions of some selected current research work on WUSNs and IoUT.

TABLE 1: Summary of the contributions of some current related works.

Reference	Contribution	Year
[27]	A new wave number model is proposed using the Peplinski principle + multiple scattering in soil medium. The path loss is modeled based on the absorption due to permittivity and multiple scattering from obstacles in soil. The path loss is then analyzed at two typical IoT frequencies of 433 MHz and 868 MHz for two proportions of VWC, 5% and 50%.	2021
[22, 28]	An IoUT architecture has been proposed to provide a total field autonomy in agriculture and to enable more efficient food production solutions through in situ monitoring, self-reporting capabilities (soil moisture, salinity, temperature, etc.), and the interconnection of existing field machinery like irrigation systems, harvesters, and seeders.	2018, 2020
[29, 30]	An acoustic-based wireless data transmission system was proposed where sensing data was transmitted over 30 m distance through soil medium.	2017, 2018
[25, 26]	To prolong the lives of energy-hungry sensor nodes in wireless sensor networks, energy management schemes are proposed to keep the sensor nodes alive. This is to make the network operational and efficient. These energy management schemes include energy harvesting, energy transfer, and energy conservation.	2018, 2021
[20]	WUSNs are used to characterize radio transmission between underground buried pipes and a base station using multilayer media. This is to identify the range of operating frequencies having lower energy loss, lower bit error rate, and power needed to transfer packets that carry data through the media.	2017
[21]	The complex refractive index model-Fresnel (CRIM-Fresnel) and the modified Fruis considered the two EM signal attenuation models for evaluating the signal strength in soil medium were reviewed, and a technique was developed to perform an experimental measurement of EM signal attenuation in the laboratory. Measured results are compared with the estimated values computed from the propagation loss models. A significant difference between the models and estimated values is established from the comparison.	2019

3. Electromagnetic Propagation through Soil

The propagation characteristics of EM in soil differ significantly from other media. This may be attributed to the properties of the soil medium which is characterized by a high attenuation factor due to high absorption and multipath losses. EM wave transmission depends largely on the dielectric constant of the material. In most cases, smaller dielectric constant values yield better transmission conditions. Soil is a dielectric material made up of air, water, and bulk soil [2]. Higher air composition and porosity in the soil promote the better performance of EM wave propagation [3]. In contrast, a high percentage of volumetric water content greatly impedes communication.

3.1. The EM Wave Transmission and Attenuation in Soil. The received signal strength or the attenuation of EM waves depends mostly on the physical properties of the soil. These properties including density, volumetric water content, and mineral content play important roles in determining the attenuation properties for the transmitted EM waves. Valuable information on the physical properties of the medium as well as the properties of the transmitted EM wave can be obtained from the received signal strength. The main contributing factor to the EM wave attenuation in the soil is the volumetric water content (VWC) of the soil [31]. The variation of the dielectric constant of the soil is determined as a function of its components [9]. The EM wave attenuation in the soil is characterized by the attenuation constant, α , and the phase shift constant β . The propagation constant or the wave number k is expressed as [32]

$$k = \sqrt{\mu\epsilon\omega^2 + i\mu\sigma\omega} = \alpha + j\beta, \quad (1)$$

where

$$\begin{aligned} \alpha = \text{Re}(k) &= \omega \sqrt{\frac{\mu\epsilon'}{2} \left[\sqrt{1 + \left(\frac{\epsilon''}{\epsilon'}\right)^2} - 1 \right]}, \\ \beta = \text{Im}(k) &= \omega \sqrt{\frac{\mu\epsilon'}{2} \left[\sqrt{1 + \left(\frac{\epsilon''}{\epsilon'}\right)^2} + 1 \right]}. \end{aligned} \quad (2)$$

In the above, σ is the electric conductivity, ϵ is permittivity, μ is the magnetic permeability of the soil, and ω is the angular frequency of the EM wave.

The additional received power losses may be attributed to the porosity of the medium, water content, pore fluid conductivity, and soil fabric. These losses are directly linked to soil properties such as the electric conductivity (σ), permittivity (ϵ), and the magnetic permeability (μ) as well as the angular frequency (ω) of the EM wave.

The electrical conductivity of soil varies widely depending on the soil type and moisture content [33].

The relative permittivity of soil arises from the interaction of the electromagnetic field with charge in the form of electric dipoles and free monopoles within the soil. Polar molecules like water absorb energy from the electric field while becoming orientated with the field. Water has a strong relative permittivity of 80 as compared to 1 for air and 5 for quartz [34]. Thus, the water content in soil strongly influences the permittivity of the soil [35]. The permittivity of a material can be expressed as [4]

$$\begin{aligned} \epsilon &= (1 + \chi_e)\epsilon_0, \\ \epsilon &= \epsilon_r\epsilon_0, \end{aligned} \quad (3)$$

where χ_e is the electric susceptibility of the medium, ϵ_r is the relative permittivity, and ϵ_0 is the permittivity of free space. The magnetic permeability of most geologic materials is the same as that of a vacuum, and it is assumed that the relative magnetic permeability for these materials is 1. But the value is different for soils that have high iron content.

3.2. EM Wave Transmission Models in Soil. EM wave transmission through soil can be modeled based on Friis' free space propagation equation, where a tweaking factor is included to account for additional losses in the soil medium. The power of the received signal, P_r in free space, is modeled as [36]

$$P_r = P_t G_t G_r \left(\frac{\lambda}{4\pi d} \right)^2, \quad (4)$$

where P_t is the transmit power, G_r and G_t are the gains of the receiver and transmitter antennas, d is the distance separating sender and receiver antennas, and λ is the EM wavelength. In decibels, Equation (4) will be expressed as [37]

$$10 \log (P_r) = 10 \log \left[P_t G_t G_r \left(\frac{\lambda}{4\pi d} \right)^2 \right], \quad (5)$$

$$10 \log (P_r) = 10 \log (P_t) + 10 \log (G_t) + 10 \log (G_r) + 20 \log \left(\frac{\lambda}{4\pi d} \right), \quad (6)$$

$$P_r = P_t + G_r + G_t - L_p, \quad (7)$$

$$L_p = L_0 + L_s \quad (\text{in dB}), \quad (8)$$

where L_0 is the path loss in free space and L_s is the additional path loss accounting for the propagation in soil. The free space path loss can be directly derived from Equation (8), without the additional path loss with $L_s = 0$ as [36]

$$L_0 = 10 \log \left(\frac{P_t}{P_r} \right) = -10 \log \left[G_t G_r \left(\frac{\lambda}{4\pi d} \right)^2 \right]. \quad (9)$$

Ignoring antenna gains, i.e., $G_r = G_t = 1$, Equation (6) is reduced to

$$L_0 = 10 \log \left(\frac{P_t}{P_r} \right) = 20 \log \left(\frac{4\pi d}{\lambda} \right). \quad (10)$$

The computation of the additional path loss L_s is performed by considering the following differences of EM wave propagation in soil compared to that in the air:

- (i) The wavelength is different based on the difference in signal velocity
- (ii) Based on the signal frequency, the wave amplitude will be different

- (iii) Color scattering and delay distortion are caused by the correlation of the phase velocity with the frequency in the soil

Hence, the additional path loss L_s in the soil can be expressed as the addition of two components

$$L_s = L_\alpha + L_\beta, \quad (11)$$

where L_α (dB) is the transmission loss due to the attenuation constant α and L_β is the attenuation loss due to the phase shift constant β . Consequently, considering that the wavelength in the soil is $\lambda_s = 2\pi/\beta$ and that of free space is $\lambda_0 = c/f$,

$$L_\beta = 20 \log \left(\frac{\lambda_0}{\lambda_s} \right), \quad (12)$$

where β as previously defined is the phase shift constant, $c = 3 \times 10^8 \text{ ms}^{-1}$, and f is the operating frequency.

Substitute the expressions of λ_s and λ_0 into Equation (12) and simplify

$$L_\beta = 154 - 20 \log (f) + 20 \log (\beta). \quad (13)$$

Since L_α is the transmission loss caused by attenuation with attenuation constant α , it can be expressed as $L_\alpha = e^{2\alpha d}$ derived from the electric field equation. When expressed in decibel, it is given by

$$L_\alpha = 20 \log (4\pi\lambda_0). \quad (14)$$

Consequently, when we substitute Equations (13) and (14) into Equation (11), the path loss of an EM wave in the soil L_p is expressed as follows:

$$L_p = 6.4 + 20 \log (d) + 20 \log (\beta) + 8.69\alpha d. \quad (15)$$

It can be seen from Figure 1 that lower frequencies are required for adequate communication in soil medium. However, reducing the operating frequency below 300 MHz will increase the antenna size, which can also prevent practical implementation of WUSNs. It is a fact that most wireless underground sensor boards like MICA2 operate within 300–400 MHz range. A suitable operating frequency range between 300 and 900 MHz will be appropriate for preserving small antenna sizes [3, 34]. This is to ensure that the sensors remain discrete, a property that is particularly useful for security applications. Figure 1 shows the graph of the path loss, L_p in decibels as a function of distance d in sandy soil with $\epsilon'_r = 4.5$ and $\epsilon'' = 0.1$ for different values of operating frequency, f . It can be seen that the path loss increases with increasing distance, d , as anticipated. Furthermore, the increase in the operating frequency, f , leads to the increase of the path loss. This analysis motivates the need to operate at lower frequencies in soil medium. This confirms the fact that the path loss is far lower for communication in free space

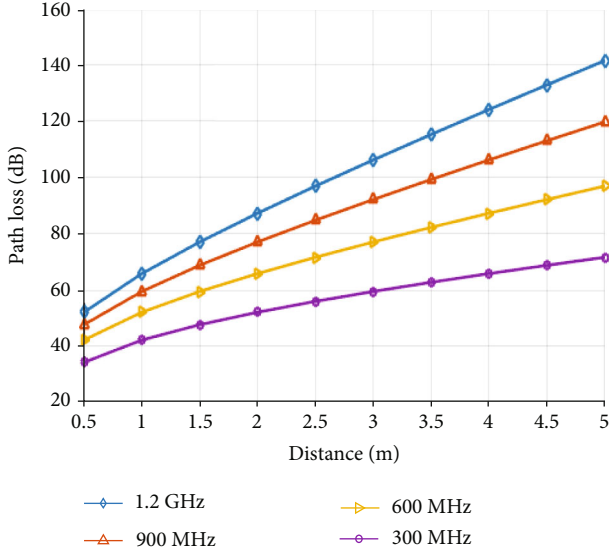


FIGURE 1: Path loss vs. distance in the soil at different frequencies.

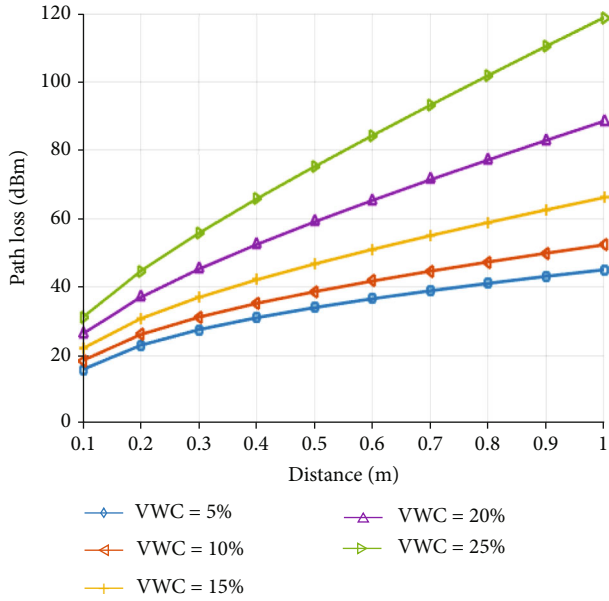


FIGURE 2: Path loss vs. distance in the soil at different VWC.

as compared to communication in soil medium. This is due to the additional path loss L_s , which is a function of the attenuation constant α and the phase shift constant β as mentioned earlier. In Figure 2, we show the effect of volumetric water content (VWC) on the path loss for values of the VWC between 5 and 25%. The path loss increases considerably with higher proportions of VWC and with the increase in distance. In Figure 3, the path loss increases even further with the increase of the frequency. A path loss increase of roughly 30 dB is possible with a VWC increase of about 20%. This effect is particularly important since water content not only depends on the location of the network but also varies during different seasons.

3.3. Underground to Above the Ground Model. The higher permittivity of soil compared to that of air results in reflection and refraction of signals that are incident to the soil-air interface. More specifically, signals can penetrate through the soil-air interface only if the incident angle is small. For underground to above the ground (UG2AG) propagation, only the waves with a small incident angle θ_i will transmit to air, as shown in Figure 4. In other words, for the UG2AG channel, the waves propagate vertically in the soil and resemble a new source at the air-soil interface.

Generally, WUSNs are deployed at depths that are less than 50 cm [38]. For the UG2AG link, due to proximity to the earth surface, a part of the EM waves propagates from soil to air, then travels along the soil-air interface, and enters the soil again to reach the receiver [39]. These EM waves called lateral waves are a major component of the underground channel. The three major contributors to the received signal strength include the direct, reflected, and lateral waves which are shown in Figure 4. The arrival time in nanoseconds of each of the three major waves contributing to EM wave attenuation in soil: the direct wave, the reflected wave, and the lateral wave, is expressed as [39]

$$\begin{aligned}\tau_d &= \left(\frac{\delta_s}{S_w}\right) + 2\left(\frac{L}{S_{\text{cox}}}\right), \\ \tau_r &= 2\left(\frac{\delta_s}{S_w}\right) + 2\left(\frac{L}{S_{\text{cox}}}\right), \\ \tau_l &= 2\left(\frac{\delta_s}{S_w}\right) + \left(\frac{\delta_a}{c}\right) + 2\left(\frac{L}{S_{\text{cox}}}\right),\end{aligned}\quad (16)$$

where δ_s is the distance traveled by the wave in the soil, L is the length of the coaxial cable attached to the antenna, S_{cox} is the speed of wave the coaxial cable calculated with the refractive index of 1.2, S_w is the speed of the wave in soil, δ_a is the distance traveled by the wave in the air, and c is the speed of light ($c = 3 \times 10^8$ m/s).

For above the ground to underground (AG2UG) channel, the refracted angle is near to zero and the propagation in the soil is also vertical. The attenuation loss due to the difference in the wavelength of the signal in soil L_β , which is also called the refraction loss for the AG2UG link, can be found as [40]

$$L_\beta = 20 \log \left(\frac{n_s \cos \theta_i + \cos \theta_t}{4 \cos \theta_i} \right), \quad (17)$$

where θ_i is the incident angle, θ_t is the refracted angle, and n_s is the refractive index of soil, which is given by

$$n_s = \left(\frac{(\epsilon' + j\epsilon'')^{1/2} + \epsilon'}{2} \right)^{1/2}, \quad (18)$$

with ϵ' and ϵ'' being the real and imaginary parts of the dielectric constant in soil.

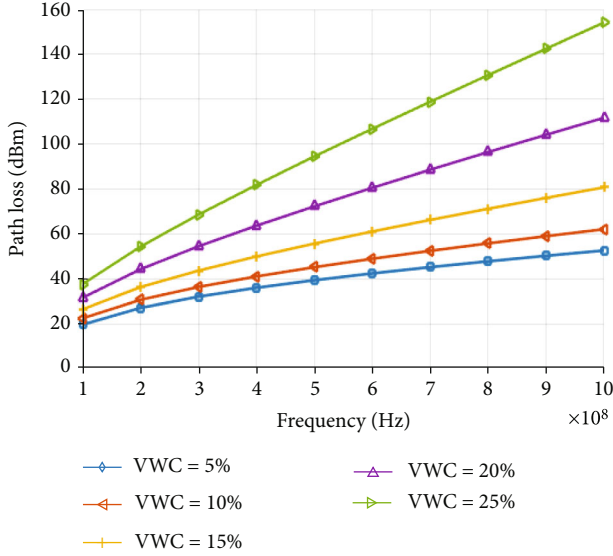


FIGURE 3: Path loss vs. frequency in the soil at different VWC.

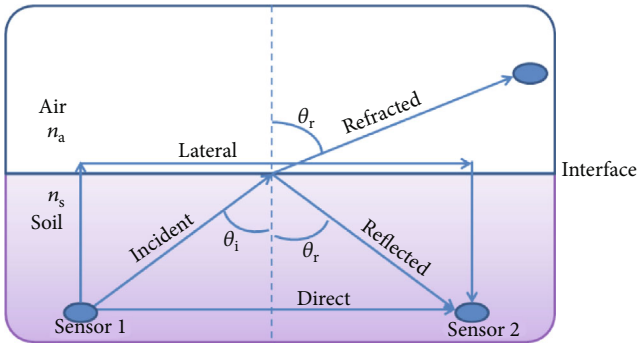


FIGURE 4: UG2AG channel model for the three EM waves' propagation.

For the AG2UG link, we consider the maximum path loss where the incident angle $\theta_i \rightarrow 0$ and $\theta_t \rightarrow 0$. Hence, L_β in Equation (17) can be approximated as

$$L_\beta = 20 \log \left(\frac{n_s + 1}{4} \right). \quad (19)$$

For the UG2AG link, the signal propagates perpendicularly from a higher density medium to a lower density one. Hence, we consider that all energy is refracted and $L_\beta = 0$.

4. Channel Capacity of EM Wave in Soil

During a wireless transmission in soil medium between the transmitter and receiver sensor nodes, the channel capacity is expressed as

$$C = B \log_2 \left(1 + \frac{S}{N_0 B} \right), \quad (20)$$

where B is the system bandwidth, S is the received signal strength (RSS) at the receiver, and N_0 is the noise power density. It is worth noting that the RSS is affected by the antenna return loss, which is given by

$$S_{dB} = P_t + 10 \log_{10} \left(1 - 10^{-(RL_{dB}/10)} \right) - L_p, \quad (21)$$

where P_t is the transmitter power, RL_{dB} is the antenna return loss, and L_p is the path loss in soil. It should be noted that all interferences are reduced to the thermal noise which is considered to be constant [41, 42].

The channel capacity and the operating frequency against soil moisture in sandy soil and clay soil are shown in Figures 5. The channel capacity in sandy soil estimated at 94.22 kbps for VWC = 10% is much higher than that of clay soil estimated at 52.86 kbps for the same proportion of VWC. In other words, sandy soil channel capacity is 78.2% higher than that of clay soil. Meanwhile, for VWC = 40%, the channel capacity of sandy soil is estimated at 307.8 kbps, which is 181.6% higher than that of clay soil estimated at 109.3 kbps. This performance is due to lower path loss in sandy soil [28, 41]. The soil type cannot be changed in practice; nevertheless, the antenna size could be modified and this can affect the behavior of the channel capacity. Figure 6 shows the frequency and the channel capacity against soil moisture for two different types of soil and at different antenna sizes of 60 mm, 100 m, and 140 mm.

5. Propagation through the Soil Using Magnetic Induction

A lot of work has been done in the area of underground magnetic induction (MI) communication. Two main deployment schemes can be identified: the direct MI transmission and the MI waveguides. The direct MI transmission has no relays deployed between sensor nodes. In comparison to the traditional wireless relaying concepts, the MI transmission solution has a lower path loss in the near and relatively far regions of transmission. As a result, the transmission range can greatly be improved compared to the EM wave-based approach for WUSNs [36]. Figure 7 shows the path losses of the MI system and EM wave system against the transmission distance at different VWC in soil [43]. It can be seen that the path loss of the MI system is a log function of the distance and the path loss of the EM wave system is a linear function of the distance. As expected, the EM wave system path loss increases vividly as VWC increases. At VWC = 1% when the soil is very dry, the path loss of the EM wave system is lower than that of the MI system. But after sufficiently long distances, MI systems achieve lower path loss. At VWC = 5% when the soil is moderately wet, the path losses of both systems are the same. It can also be observed in the near region (between 0.3 m and 3 m) that the EM wave system has a smaller path loss. In the relatively far region (a distance greater than 3 m), the MI system shows a smaller path loss than the EM wave system. When the soil is very wet, i.e., at VWC = 25%, the path loss of the EM wave system is considerably greater than that of the MI system.

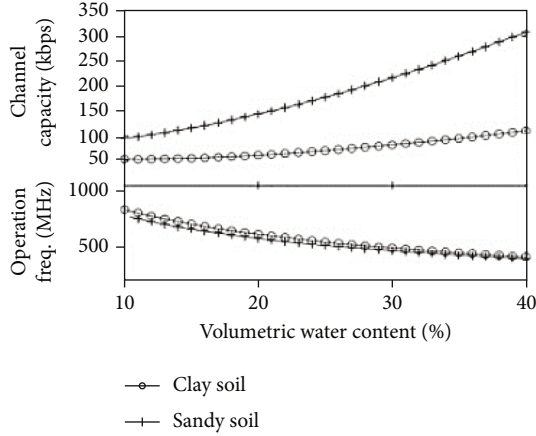


FIGURE 5: Channel capacity and frequency at different soil types [41].

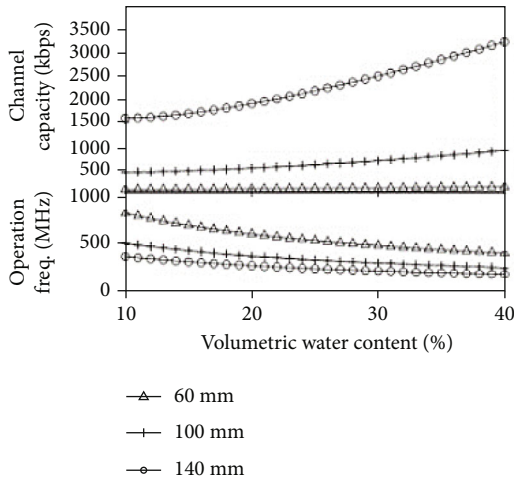


FIGURE 6: Channel capacity and frequency at different antenna sizes [41].

Table 2 presents the comparison of the three most common technologies of wireless sensor networks used for the implementation of IoUT.

5.1. Direct Magnetic Induction Propagation Models. Since all signal mappings involved in MI transmission are linear, a linear channel model should be adopted. The waveguide may be viewed as a chain of circuits made up of capacitors, resistors, and inductors. The capacitance of the capacitor is chosen to make each circuit resonate at frequency f_0 [2].

The effect of eddy currents leads to an exponential decrease of the field strength with the transmission distance. Hence, the loss factor G can be expressed as [4]

$$G = \exp\left(-\frac{r}{\delta}\right), \quad (22)$$

where δ is the skin depth, which depends on the signal frequency, conductivity, and permittivity of soil. In a two-

dimensional space, the polarization factor is expressed as [6]

$$J = 2 \sin(\theta_t) \sin(\theta_r) + \cos(\theta_t) \cos(\theta_r), \quad (23)$$

where θ_t and θ_r are the transmitting and receiving angles, respectively.

Direct magnetic induction propagation is the process where signals are transmitted and received through the use of a coil of wires. Figure 8 shows two coils in communication, where a_t is the radius of the transmitting coil, a_r the radius of the receiving coil, and r is the distance between the transmitter and the receiver [2].

The important signal propagation effects such as attenuation, signal reflections, and frequency splitting in the direct MI communication channels can be expressed as a path loss function [5].

5.2. Propagation Model Using Magnetic Induction Waveguide. A diagram of an MI waveguide with a transmitter, a receiver, and $(k-1)$ relays is shown in Figure 9.

The magnetic induction waveguide structure as shown in Figure 9 is made up of a transmitter circuit with a voltage source U_t , a receiver circuit with a load impedance Z_L , and $(k-1)$ passive relays. These circuits are placed at equal distances between the transceivers. Each circuit includes a magnetic antenna, a capacitor with capacitance C , an inductor with inductance L , and a resistor with resistance R .

5.3. Interference in Magnetic Induction Propagation. In direct MI transmission WUSNs, the sources of interference in the circuits of the nearby devices including the transmitter can be ignored due to a high path loss [5], such that only the interference produced in the receiver circuit needs to be taken into consideration. According to MI waveguide performance evaluation, the received interference power at the load impedance is necessary but thermal noise is assumed to be the dominant source of interference [35]. It is worth noting that this interference is caused by the resistors in the relay and the transceiver circuits. Meanwhile, the potential difference of the noise from resistor R in each relay is modeled as a supplementary voltage source. The received noise power at the load resistor is computed as the addition of the received noise power caused by the copper resistance of the coils including the transceiver coils and the received noise power produced by the load resistor. This is performed according to the superposition principle [4].

6. Acoustic-Based Wireless Transmission in Soil Medium

A lot of research work has been done in wireless underground communication systems based on acoustic wave transmission to support many applications. Depending on the signal generation, the acoustic-based techniques can be categorized into passive and active kinds of techniques. In the passive acoustic-driven technique, natural events such as volcano explosions, nuclear explosions, and earthquakes in the subterranean environment cause acoustic signals. Then, sensors placed in this vicinity detect infrasonic signals

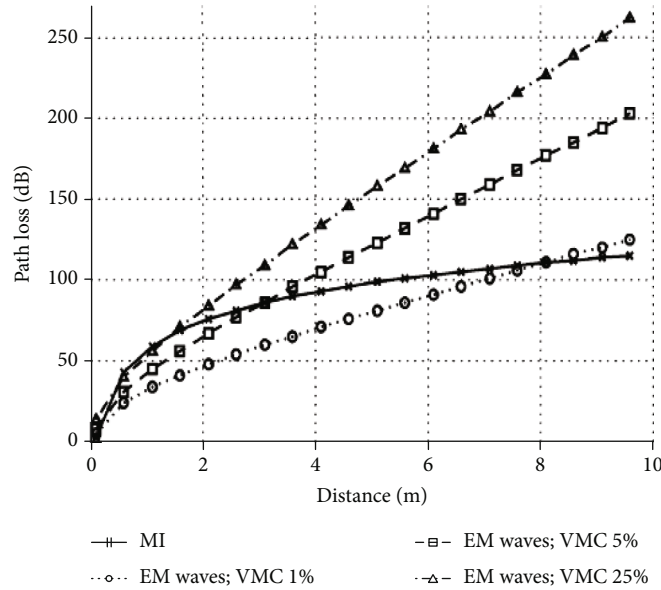


FIGURE 7: Path losses of the MI system and EM wave system with different VWC in soil [43].

TABLE 2: Comparison between IoUT communication technologies: EM, MI, and acoustic.

Parameters	EM	MI	Acoustic
Transmission range	Few meters	In 10s of meters	In 100s of meters
Attenuation	High	Low	High
Interference	High	Low	Medium
Installation cost	Moderate	Medium	Medium
Data rate	In bps	In kbps	In 10s of bps
Application	Agriculture, seismic exploration, intrusion detection, buried pipeline monitoring (oil and gas, water), downhole telemetry	Downhole telemetry	Seismic exploration, buried pipeline monitoring, downhole telemetry
Advantages	High data rate compared to acoustic systems, easy to install, support multihop communication	The high data rate, low attenuation, and support multihop communication	High data rate compared to MPT systems, long transmission range
Disadvantages	High attenuation and interference, limited transmission range, and requires a large antenna	The orientation between coils is required; limited transmission range needs dense deployment	High attenuation and lower data rate than EM and MI

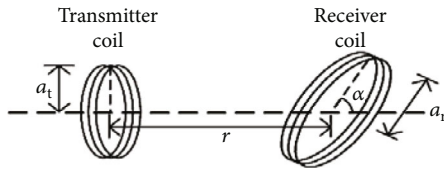


FIGURE 8: Direct MI transmission.

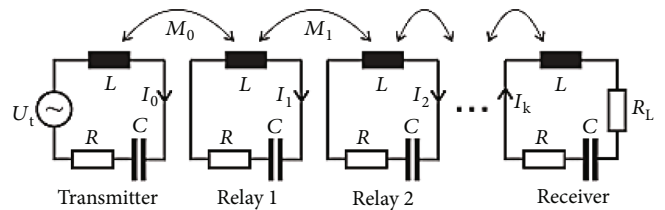


FIGURE 9: MI waveguide with transmitter diagram with transmitter, receiver, and $(k - 1)$ relays.

which are useful for the prediction of natural disasters. This technique can also be used to detect underground pipeline leakage. In the active acoustic-driven technique, an artificial explosion or vibration is used for the generation of signals which are sent underground to estimate the properties of reflection-based seismology. Acoustic waves are mostly used

for detection purposes in soil medium rather than for communication. This is because of the low propagation speed of these waves in the soil medium. In [29, 30], an acoustic-based wireless data transmission system was proposed where

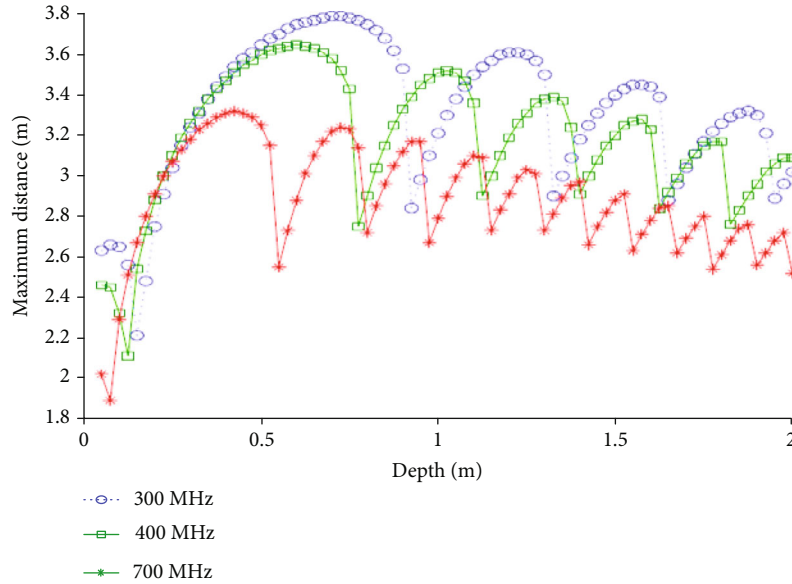


FIGURE 10: Maximum internode distance as a function depth for different operating frequencies [3].

sensing data was transmitted over 30 m distance through soil medium. In [44], a soil equation was derived for the propagation of acoustic waves in soil medium at the frequency of 16 kHz. Furthermore, acoustic waves at 900 Hz frequency was used for the estimation of the moisture content of the soil [45]. Acoustic waves are also commonly used for downhole telemetry purposes.

7. Research Challenges

WUSN promises a new future in agriculture, security, etc., but for us to derive those benefits, several challenges still need to be overcome. Whilst underground tunnels have been investigated in the past, very little is known about direct propagation in soil medium. To realize the promised benefits, a concerted effort is required on the part of researchers to address some of the outstanding issues.

7.1. Challenges of WUSNs in Soil Medium Using EM Waves

7.1.1. Limited Communication Range. Research has shown that the maximum attainable communication range and the reliability of wireless links in the underground environment are much more constrained as compared to over-the-air wireless sensor networks. As a result of these factors, multi-hop communication should be considered in the design of WUSN topology.

7.1.2. Soil Properties. Soil properties have a direct influence on the wireless sensor network performance. Transmission quality is greatly hampered by the increase of water content in the soil. So therefore, the design of network topology must be robust enough to adapt to changes in channel conditions.

7.1.3. Topology Design. It is important to carefully examine the composition of the soil at a specific location to adapt

the topology design according to the exact characteristics of the soil channel at that location [2].

7.1.4. Depths of Buried Sensor Nodes. EM wave transmission in soil medium is also affected by the changes in depths of buried sensor nodes. With the effect of reflection in a two-path channel model, there are fluctuations in the maximum internode distance as the bury depth increases as shown in Figure 10 [3]. Consequently, at various depths in the soil, diverse ranges of transmission distance can be achieved. Therefore, an optimal strategy for providing connectivity and coverage is required to design a well-structured topology that is adaptive to the effects of the channel.

7.1.5. Operating Frequency. Signal attenuation in soil has been very well illustrated by the WUSN channel model, and this is due to an increase in functional frequency. Studies have proven that it is important to deploy wireless sensor networks at low frequencies for efficient signal transmission. Nevertheless, signal propagation at smaller frequencies will lead to a trade-off between the antenna size and the frequency. Figure 10 [3] shows the internode distance as a function of bury depth of sensor nodes at a specific operating frequency. This graph describes the maximum sensor depths mapped to a maximum internode distance. Based on the analysis of the graph, the deployment of wireless sensor networks in the soil must be adapted to a specific operating frequency of the sensors. It should also be noted that the performance of transmission at low depths discloses the fact that using a static frequency is not promoting the best performance for WUSNs. Some other studies have suggested cognitive radio techniques where adaptive operations could be applied to wireless sensor networks in soil medium [14].

7.1.6. Environmental Conditions. Environmental circumstances are also a determining factor for wireless sensor network quality. Climatic and seasonal alterations resulting in

the variation of soil moisture content coupled with the effects of soil type significantly affect the performance of the signal transmission. So, therefore, environmental dynamics should be taken into account during the design of protocols for wireless sensor networks in the soil. Cognitive techniques could be applied for the design of environment aware protocols that can adapt to functional parameters of the area of deployment. Besides, the direct impact and the dynamic nature of the physical layer so far as transmission quality is concerned make it imperative for new crosslayer design processes adaptive to the changes in the environment for wireless sensor networks in soil [7].

7.2. Challenges of WUSNs in Soil Medium Using Magnetic Induction Waveguide. The communication range of the magnetic induction waveguide technique which is around 10 m is still limited. This could be improved through further research work. The magnetic induction method resolves the difficulties of deploying sensor nodes with large antenna size and dynamic channel situation encountered in the electromagnetic wave transmission method. The path loss is also reduced by half when using the magnetic induction technique in comparison to the EM wave transmission method. Nevertheless, communication by multiple hopping among sensor nodes remains relevant during the implementation of the magnetic induction method. More so, there is the need for the deployment of multiple relay coils between the transmitters and receivers. It is worth noting that the deployment of the coils in this setup is labor-intensive even though the relay coils consume less energy and are cost-effective. It is therefore important to take into account the factors mentioned above during the structural design of the network topology.

The magnetic induction waveguide also adopts a complex three-dimensional structural network topology. As a consequence, the relay coils in diverse communication networks would affect each other in a three-dimensional space. Hence, the necessity to develop a multiple-hop channel model in a three-dimension network for the wireless communication of sensor nodes in that kind of configuration [2].

8. Conclusion

A review of underground wireless channel models is presented. WUSNs can be modeled in soil medium taking into account the properties of soil. Channel models for EM, MI, and acoustic signal transmission through soil medium are described. A comparative table of these transmission techniques is also provided to establish the differences between them. EM signal propagation in soil was analyzed based on the path loss and channel capacity at a different volumetric water content of the soil. It is concluded that EM signals perform better at lower frequencies and in dry sandy soil. MI waveguide is described as a wireless communication technique in soil medium for certain applications. Path loss graphs for EM and MI have been provided to compare the performance of these techniques in soil medium. It has also been established that acoustic-based propagation is commonly used for detection purposes rather than communica-

tion purposes because of the low propagation speed of this technique in soil. Some critical research challenges for WUSNs are identified. An alternative approach that could be suggested to improve upon the performance of such systems is to consider the use of small hollow tunnels, which are buried in the soil. Such tunnels will have the advantage of providing communication characteristics of the air environment as such can help in overcoming some of the challenges of direct communication in soil.

Data Availability

Previously reported data were used to support this study and these prior studies and datasets are cited at relevant places within the article.

Conflicts of Interest

The authors declare that there is no conflict of interest regarding the publication of this paper.

Acknowledgments

The authors acknowledge Laboratoire Ondes et Milieux complexes (LOMC) UMR CNRS 6294, University of Le Havre, France; the Department of Computer Science at the University of Ghana; and the Department of Information Technology, UPSA, for their support.

References

- [1] K. Arshad, F. Katsriku, and A. Lasebae, "Modeling obstructions in straight and curved rectangular tunnels by finite element approach," *Journal of Electrical Engineering*, vol. 9, no. 1, pp. 9–13, 2008.
- [2] I. F. Akyildiz, Z. Sun, and M. C. Vuran, "Signal propagation techniques for wireless underground communication networks," *Physical Communication*, vol. 2, no. 3, pp. 167–183, 2009.
- [3] M. C. Vuran and I. F. Akyildiz, "Channel model and analysis for wireless underground sensor networks in soil medium," *Physical Communication*, vol. 3, no. 4, pp. 245–254, 2010.
- [4] S. Kisseleff, W. Gerstacker, R. Schober, Z. Sun, and I. F. Akyildiz, "Channel capacity of magnetic induction based wireless underground sensor networks under practical constraints," in *2013 IEEE Wireless Communications and Networking Conference (WCNC)*, Shanghai, China, April 2013.
- [5] S. Kisseleff, I. F. Akyildiz, and W. H. Gerstacker, "Throughput of the magnetic induction based wireless underground sensor networks: key optimization techniques," *IEEE Transactions on Communications*, vol. 62, no. 12, pp. 4426–4439, 2014.
- [6] Z. Sun and I. F. Akyildiz, "On capacity of magnetic induction-based wireless underground sensor networks," in *2012 Proceedings IEEE INFOCOM*, Orlando, FL, USA, March 2012.
- [7] K. Arshad, F. Katsriku, and A. Lasebae, "Effect of different parameter on attenuation rate in circular and arch tunnels," *PIERS Online*, vol. 3, no. 5, pp. 607–611, 2006.
- [8] K. Martinez, R. Ong, and J. Hart, "Glacsweb: a sensor network for hostile environments," in *2004 First Annual IEEE Communications Society Conference on Sensor and Ad Hoc*

- Communications and Networks, 2004. IEEE SECON 2004*, pp. 81–87, Santa Clara, CA, USA, October 2004.
- [9] L. Li, M. C. Vuran, and I. F. Akyildiz, “Characteristics of the underground channel for wireless underground sensor networks,” in *The Sixth Annual Mediterranean Ad Hoc Networking WorkShop*, Corfu, Greece, June 2007.
 - [10] Z. Sun and I. F. Akyildiz, “Channel modeling and analysis for wireless networks in underground mines and road tunnels,” *IEEE Transactions on Communications*, vol. 58, no. 6, pp. 1758–1768, 2010.
 - [11] T. P. Weldon and A. Y. Rathore, “Wave propagation model and simulations for landmine detection,” Tech. Rep., University of North Carolina-Charlotte, 1999.
 - [12] J. Wait and J. Fuller, “On radio propagation through earth,” *IEEE Transactions on Antennas and Propagation*, vol. 19, no. 6, pp. 796–798, 1971.
 - [13] D. J. Daniels, “Surface-penetrating radar,” *Electronics & Communication Engineering Journal*, vol. 8, no. 4, pp. 165–182, 1996.
 - [14] I. F. Akyildiz, W. Y. Lee, M. C. Vuran, and S. Mohanty, “Next generation/dynamic spectrum access/cognitive radio wireless networks, a survey,” *Computer Networks Journal*, vol. 50, no. 13, pp. 2127–2159, 2006.
 - [15] A. Chehri, P. Fortier, and P. M. Tardif, “Security monitoring using wireless sensor networks,” in *Fifth Annual Conference on Communication Networks and Services Research (CNSR '07)*, pp. 13–17, Fredericton, NB, Canada, May 2007.
 - [16] G. A. Kennedy and P. J. Foster, “High resilience networks and microwave propagation in underground mines,” in *2006 European Conference on Wireless Technology*, pp. 193–196, Manchester, UK, September 2006.
 - [17] J. F. Mastarone and W. J. Chappell, “Urban sensor networking using thick slots in manhole covers,” in *2006 IEEE Antennas and Propagation Society International Symposium*, pp. 779–782, Albuquerque, NM, USA, July 2006.
 - [18] N. Elkmann, H. Althoff, S. Kutzner, T. Stuerze, J. Saenz, and B. Reimann, “Development of fully automatic inspection systems for large underground concrete pipes partially filled with wastewater,” in *Proceedings 2007 IEEE International Conference on Robotics and Automation*, pp. 130–135, Rome, Italy, April 2007.
 - [19] M. A. Akkas and R. Sokullu, “Wireless underground sensor networks: channel modeling and operation analysis in the terahertz band,” *International Journal of Antennas and Propagation*, vol. 2015, Article ID 780235, 12 pages, 2015.
 - [20] S. Mekid, D. Wu, R. Hussain, and K. Youcef-Toumi, “Channel modeling and testing of wireless transmission for underground in-pipe leak and material loss detection,” *International Journal of Distributed Sensor Networks*, vol. 13, no. 11, Article ID 155014771774471, 2017.
 - [21] D. Abdorahimi and A. M. Sadeghioon, “Comparison of radio frequency path loss models in soil for wireless underground sensor networks,” *Journal of Sensors and Actuator Network*, vol. 8, no. 2, p. 35, 2019.
 - [22] M. C. Vuran, A. Salam, R. Wong, and S. Irmak, “Internet of underground things in precision agriculture: architecture and technology aspects,” *Ad Hoc Networks*, vol. 81, no. 1, pp. 160–173, 2018.
 - [23] U. Raza and A. Salam, *Wireless Underground Communications in Sewer and Stormwater Overflow Monitoring: Radio Waves through Soil and Asphalt Medium*, Springer International Publishing, Cham, Switzerland, 2020.
 - [24] N. Saeed, M.-S. Alouini, and T. Y. Al-Naffouri, “Toward the Internet of Underground Things: a systematic survey,” *IEEE Communication Survey & Tutorials*, vol. 21, no. 4, pp. 3443–3466, 2019.
 - [25] F. Engmann, F. A. Katsriku, J.-D. Abdulai, K. S. Adu-Manu, and F. K. Banaseka, “Prolonging the lifetime of wireless sensor networks: a review of current techniques,” *Wireless Communications and Mobile Computing*, vol. 2018, Article ID 8035065, 23 pages, 2018.
 - [26] F. Engmann, K. S. Adu-Manu, J.-D. Abdulai, and F. A. Katsriku, “Applications in prediction approaches in wireless sensor networks,” in *Wireless Sensor Network-Design, Deployment and Applications*, IntechOpen, 2021.
 - [27] F. K. Banaseka, H. Franklin, F. Katsriku, J.-D. Abdulai, A. Ekpezu, and I. Wiafe, “Soil medium electromagnetic scattering model for the study of wireless underground sensor networks,” *Wireless Communications and Mobile Computing*, vol. 2021, Article ID 8842508, 11 pages, 2021.
 - [28] A. Salam, *Internet of things in agricultural innovation and security*, Springer, Cham, 2020.
 - [29] A. Singer, S. Yang, and M. Oelze, “Acoustic communications: through soils, sands, water, and tissue,” *The Journal of the Acoustical Society of America*, vol. 141, no. 5, pp. 3986–3987, 2017.
 - [30] S. Yang, O. Baltaji, Y. M. Hashash, and A. Singer, “Soilcomm: a miniaturized through-soil wireless data transmission system,” *The Journal of the Acoustical Society of America*, vol. 144, no. 3, pp. 1872–1872, 2018.
 - [31] M. C. Vuran and A. R. Silva, “Communication through soil in wireless underground sensor networks—theory and practice,” in *Sensor Networks. Signals and Communication Technology*, G. Ferrari, Ed., Springer, Berlin, Heidelberg, 2010.
 - [32] D. K. Cheng, *Field and Wave Electromagnetic*, Addison-Wesley, Reading, MA, USA, 2nd edition, 1989.
 - [33] R. Grisso, M. M. Alley, D. L. Holshouser, and W. E. Thomason, *Precision Farming Tools: Soil Electrical Conductivity*, Virginia Cooperative Extension, 2009.
 - [34] I. F. Akyildiz and E. P. Stuntebeck, “Wireless underground sensor networks: research challenges,” *Ad Hoc Networks*, vol. 4, no. 6, pp. 669–686, 2006.
 - [35] K. Lee and D.-H. Cho, “Maximizing the capacity of magnetic induction communication for embedded sensor networks in strongly and loosely coupled regions,” *IEEE Transactions on Magnetics*, vol. 49, no. 9, pp. 5055–5062, 2013.
 - [36] A. R. Silva and M. C. Vuran, “Empirical evaluation of wireless underground-to-underground communication in wireless underground sensor networks,” in *Distributed Computing in Sensor Systems. DCOSS 2009. Lecture Notes in Computer Science, vol 5516*, B. Krishnamachari, S. Suri, W. Heinzelman, and U. Mitra, Eds., Springer, Berlin, Heidelberg, 2009.
 - [37] Y. S. Cho, J. Kim, W. Y. Yang, and C. G. Kang, “MIMO-OFDM wireless communication with MATLAB,” IEEE Press, John Wiley & Sons (Asia) Pte Ltd, 2010.
 - [38] H. R. Bogena, M. Herbst, J. A. Huisman, U. Rosenbaum, A. Weuthen, and H. Vereecken, “Potential of wireless sensor networks for measuring soil water content variability,” *Vadose Zone Journal*, vol. 9, no. 4, pp. 1002–1013, 2010.
 - [39] W. P. King, M. Owens, and T. T. Wu, *Lateral Electromagnetic Waves*, Springer-Verlag, 1992.
 - [40] A. Salam and M. C. Vuran, “Pulses in the sand: impulse response analysis of wireless underground channel,” in *IEEE*

INFOCOM 2016 - The 35th Annual IEEE International Conference on Computer Communications, San Francisco, CA, USA, April 2016.

- [41] A. Salam and U. Raza, "Underground wireless channel bandwidth and capacity," in *Signals in the Soil*, Springer, Cham, 2020.
- [42] A. Salam, "Design of subsurface phased array antennas for digital agriculture applications," in *2019 IEEE International Symposium on Phased Array System & Technology (PAST)*, Waltham, MA, USA, October 2019.
- [43] Z. Sun and I. F. Akyildiz, "Magnetic induction communications for wireless underground sensor networks," *IEEE Transactions on Antennas and Propagation*, vol. 58, no. 7, pp. 2426–2435, 2010.
- [44] R. Freire, M. H. M. de Abreu, R. Y. Okada, P. F. Soares, and C. R. Granhen Tavares, "Sound absorption coefficient in situ: an alternative for estimating soil loss factors," *Ultrasonics Sonochemistry*, vol. 22, pp. 100–107, 2015.
- [45] R. Sharma and A. Gupta, "Continuous-wave acoustic method for determination of moisture content in agricultural soil," *Computers and Electronics in Agriculture*, vol. 73, no. 2, pp. 105–111, 2010.

Research Article

Optimal Sensor Placement for Underground Tunnel Monitoring via Wireless Sensor Networks

Yonggang Li¹, Bin He,² and Youming Wang¹

¹Department of automation, Xi'an University of Posts and Telecommunications, Xi'an, 710121, China

²Electrical Engineering Department, Tongji University, Shanghai 200092, China

Correspondence should be addressed to Yonggang Li; activebee1979@163.com

Received 15 October 2020; Revised 22 November 2020; Accepted 11 December 2020; Published 29 January 2021

Academic Editor: Jose M. Gimenez-Guzman

Copyright © 2021 Yonggang Li et al. This is an open access article distributed under the Creative Commons Attribution License, which permits unrestricted use, distribution, and reproduction in any medium, provided the original work is properly cited.

In replace of human labor, wireless sensor networks (WSNs) are increasingly being utilized to perform structural health monitoring of underground tunnel. Due to its complex environment, the deployment of sensor nodes poses a big challenge to related staff. How to use the optimal number of sensor nodes deployed in the underground tunnel to obtain a satisfactory monitoring is our main consideration. In this paper, we propose a deployment strategy based on the optimal index to provide guidelines for sensor node placement. The objective of the strategy is to put sensor nodes in a proper site to gain maximum sensing information, thus eliminating redundant sensor nodes as well as saving costs.

1. Introduction

Sensor node placement should meet two basic requirements: coverage and connectivity. Sensor nodes deployed in a sensing field have the ability to sense and display the full information of objects. Even if there appear many kinds of holes such as coverage holes, routing holes, jamming holes, and wormholes in a specified region of interest, related sensor nodes depend on self-healing algorithms to detect and recover these holes in order to achieve the full coverage [1–3]. Moreover, sensor nodes are required to communicate with each other, thus making the delivery of the sensing information possible. A network is said to be fully multihop connected if it has at least one wireless multihop path linking each sensor node to each other sensor node. Especially in the presence of sensor failures, a network still remains connected relying on some connectivity modes of WSNs [4–6]. Coverage and connectivity together are two fundamental metrics to evaluate the performance of WSNs [7, 8].

There is growing interest in deploying wireless sensors in the underground tunnel to perform structural health monitoring including damage detection, crack detection, and water leakage detection [9, 10]. However, a complex under-

ground environment brings a considerable difficulty in deploying sensor nodes. Gupta et al. reviewed the following optimization criteria for optimal placement of piezoelectric sensors and actuators on a smart structure such as maximizing modal forces/moments, maximizing degree of controllability/observability, and minimizing spill-over effects [11]. Nestorovic and Trajkov developed a general approach to optimal actuator and sensor placement applicable for beam and plate structures as well as other complex geometries of structures, which has advantage over modal truncation and mathematical criteria due to its selection of the modes of interest [12]. Following the line of this research, we expand the scenario from the beam and plate structures to the underground environment. This paper attaches importance to optimization criteria based on H_2 and H_∞ norms, which are calculated for all possible candidate locations.

The remainder of this paper is organized as follows. Section 2 points out sensor deployment issues existing in placement process. Section 3 is concerned with the state space of the underground tunnel. The optimal placement index is derived based on the balanced model reduction of state space. In Section 4, the placement case of the underground tunnel based on the optimal placement index is proposed to gain

insight into sensor node deployment. Finally, the paper is concluded in Section 5.

2. Sensor Node Deployment Issue

A disk model is adopted that a sensor has a fixed sensing radius, and sensing area is characterized by a regular disk [13]. Furthermore, it is assumed that everything with this area can be perfectly observed, and everything outside cannot be measured by the sensors. If sensor nodes are densely deployed in sensor field, sensing areas of sensor nodes are overlapped, thus producing redundant reformation in WSNs (see Figure 1(a)). On the other hand, if sensor nodes are sparsely deployed in the sensor field, sensing areas of sensor nodes are independent of each other, thus causing unsatisfactory coverage (see Figure 1(c)). The purpose of optimal sensor node is to achieve the maximum sensing information using the minimum number of sensors deployed in sensor field.

Let S denotes the sensor area of a sensor, subscripts i and j represent different sensors, and r the radius of sensor area, $S(x_i, y_j)$ be spatial coordinates of sensor i . The three relationships of sensor node deployment are expressed as follows:

$$\begin{cases} S_i \cap S_j = S_c, & \text{if } \sqrt{(x_i - x_j)^2 + (y_i - y_j)^2} < 2r \\ S_i \cap S_j = c, & \text{if } \sqrt{(x_i - x_j)^2 + (y_i - y_j)^2} = 2r \\ S_i \cap S_j = \varnothing, & \text{if } \sqrt{(x_i - x_j)^2 + (y_i - y_j)^2} > 2r \end{cases}, \quad (1)$$

where S_c represents the overlapping region between two sensor sensing areas, c represents the point of contact. Let the whole area of an event area be Q , and the number of sensors n should satisfy the following inequality:

$$n > \frac{Q}{S}. \quad (2)$$

3. Theoretical Derivation

3.1. State Space of the Underground Tunnel. The equation of motion of the underground tunnel can be approximately expressed as follows:

$$M\ddot{q} + D_d\dot{q} + Kq = F, \quad (3)$$

where M represents the mass matrix, D_d the damping matrix, and K the stiffness matrix. The vector q contains all node-wise control forces F_C :

$$q^T = [u_1^T \ \phi_1 \ u_2^T \ \phi_2 \ \cdots \ u_n^T \ \phi_n]. \quad (4)$$

The total load vector F is split for the purpose of the control design into the vector of external forces F_E and the vector of the control forces F_C :

$$F = F_E + F_C = \bar{E}\bar{f}(t) + \bar{B}\bar{u}(t) = B_0u, \quad (5)$$

where matrix B_0 represents the input matrix, and vector u includes all model inputs. For the controller design purposes, Eq. (3) is accompanied by the output equation in the form

$$y = C_{0q}q + C_{0v}\dot{q}, \quad (6)$$

where in general case C_{0q} represents the output displacement matrix, C_{0v} represents the output velocity matrix, and q is the generalized displacement vector containing all degrees of freedom. Solution of Eq. (3) is determined in the form $q = \varphi e^{j\omega t}$ by solving the eigenvalue problem for a homogeneous case

$$\det(K - \omega^2 M) = 0, \quad (7)$$

where ω_i is the i th natural frequency and φ_i is the i th mode shape vector. The solution can be represented in the matrix form by the matrix of natural eigenfrequencies Ω and the modal matrix Φ .

$$\Omega = \begin{bmatrix} \omega_1 & 0 & \cdots & 0 \\ 0 & \omega_2 & \cdots & 0 \\ \cdots & \cdots & \ddots & \cdots \\ 0 & 0 & \cdots & \omega_n \end{bmatrix},$$

$$\Phi = \begin{bmatrix} \varphi_{11} & \varphi_{12} & \cdots & \varphi_{n1} \\ \varphi_{12} & \varphi_{22} & \cdots & \varphi_{n2} \\ \cdots & \cdots & \ddots & \cdots \\ \varphi_{1n_{dof}} & \varphi_{1n_{dof}} & \cdots & \varphi_{1n_{dof}} \end{bmatrix} = [\varphi_1 \ \varphi_2 \ \cdots \ \varphi_n]. \quad (8)$$

The nodal model representation (3) is transformed into a model in modal coordinates applying the following modal transformation:

$$q = \Phi q_m, \quad (9)$$

where q_m represents the vector of modal degrees of freedom or generalized modal displacements. Since the mass and the stiffness matrix are symmetric and positive definite, it can be shown that the mode shapes corresponding to distinct natural frequencies are orthogonal with respect to mass and stiffness matrix

$$\Phi^T M \Phi = M_m = \text{diag}(m_i), \quad \Phi^T K \Phi = K_m = \text{diag}(m_i \omega_i^2). \quad (10)$$

After appropriate transformations taking into account the orthogonality [13], the modal model is obtained in the form of a system of decoupled equations under the assumption of proportional damping in (4)

$$D_d = \alpha M + \beta K. \quad (11)$$

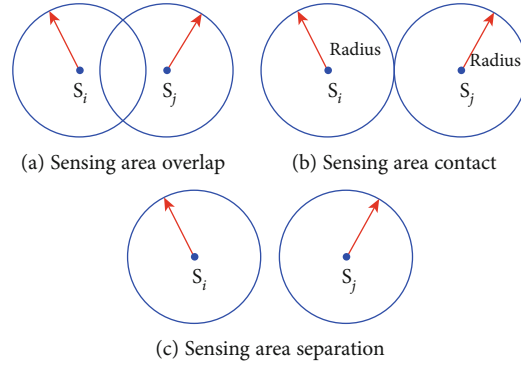


FIGURE 1: Sensor node deployment.

By appropriate selection of the state-space vector, the state-space models of different forms can be obtained. With the coordinate transformation in the state-space form

$$x = \begin{bmatrix} \Omega q_m \\ \dot{q}_m \end{bmatrix}, \quad (12)$$

$$\begin{cases} \dot{x} = Ax + Bu \\ y = Cx + Du \end{cases}. \quad (13)$$

Coefficient matrices are expressed as follows:

$$A = \begin{bmatrix} 0 & \Omega \\ -\Omega & -2z\Omega \end{bmatrix}, B = \begin{bmatrix} 0 \\ B_m \end{bmatrix}, C = [C_{mq} \quad C_{mv}], D = 0, \quad (14)$$

where $\Omega^2 = M_m^{-1}K_m$, $Z = \text{diag}(\zeta_i)$ with ζ_i being the damping ratio of the i th mode, $B_m = \Phi^T B_0$, $C_{mq} = C_{0q}\Phi$, and $C_{mv} = C_{0v}\Phi$.

Considering that flexible structures can be described in terms of independent coordinates, the modal state-space model can be expressed in terms of state-space realizations (A_{mi}, B_{mi}, C_{mi}) for each mode i , with the coordinate transformation corresponding to (12)

$$x_i = \begin{bmatrix} \omega_i \dot{q}_m \\ q_m \end{bmatrix}. \quad (15)$$

Corresponding matrices in the realization (A_{mi}, B_{mi}, C_{mi}) are determined

$$A_{mi} = \begin{bmatrix} 0 & \omega_i \\ -\omega_i & -2\xi_i\omega_i \end{bmatrix}, B_{mi} = \begin{bmatrix} 0 \\ b_{mi} \end{bmatrix}, C_{mi} = \begin{bmatrix} C_{mq_i} & C_{mv_i} \\ \omega_i & \end{bmatrix}. \quad (16)$$

The elements of the realization (A_{mi}, B_{mi}, C_{mi}) are used for assessing the optimal sensor locations based on candidate input/output transfer functions relating corresponding sensor.

3.2. Balanced Model Reduction. It is well known that the general modeling problem involves a tradeoff between complexity and accuracy of models. Simple and accurate models have the advantage over complex and inaccurate models in that the former has more rich descriptive and predictive power than the latter. So how to obtain a simple model with the same properties as the original model is the core work of model reduction.

Model reduction of large-scale dynamical systems has received a lot of attention during the last two decades. It is a crucial tool in reducing the computational complexity while preserving the properties of the original systems. It has been widely applied in many applications such as VLSI Circuits and weather forecasting.

Model reduction for linear systems is well developed based on several years of research work and intrinsic properties of linear systems. While extended to nonlinear systems, some considerations must be confronted. Thus, model reduction for nonlinear systems is much more difficult than that for linear systems. The difficulty involved in the model reduction for nonlinear systems comes from the following two facts. One is that nonlinear systems exhibit more complex behaviors than linear systems in the sense that the reduced models for nonlinear systems need to preserve much nonlinear properties. The other is that it is hard to obtain a general and universal input-output representation similar to the transfer function to describe nonlinear systems. Lack of representation adds the corresponding burden to the nonlinear system model reduction work.

Model reduction via balancing is gaining popularity because of its simple implement and clear presentation. Balancing is a well-known subject which dated back to a paper of Moor with the aim of using it to cope with model reduction [14]. If a linear system is in balanced form, the Hankel singular value acts as a tool to measure the influence of the corresponding state component on the output and input energy. If

a Hankel singular value is relatively small, the impact of the corresponding state component on the output and input energy is small. Some state components corresponding to relatively large Hankel singular value are regained, and some others corresponding to relatively small Hankel singular value are eliminated, thus forming a reduced-order model. Here, a linear time-invariant system is illustrated to be familiar with the balancing model reduction.

For a linear continuous invariant system, the state-space form is given by Eq. (17).

$$\begin{cases} \dot{x} = Ax + Bu \\ y = Cx \end{cases} \quad (17)$$

Reachability gramian and observability gramian which correspond to the above system are given by Eq. (4), respectively. If the system is stable and controllable, then the controllability gramian has full rank. Likewise, if the system is observable, then the observability gramian has full rank.

$$\begin{cases} P = \int_0^{\infty} e^{At} BB^T e^{At} dt \\ Q = \int_0^{\infty} e^{A^T t} C^T C e^{A^T t} dt \end{cases} \quad (18)$$

The reachability gramian and observability gramian satisfy the following Lyapunov equation given by (19).

$$\begin{cases} AP + PA^T + BB^T = 0 \\ QA + A^T Q + C^T C = 0 \end{cases} \quad (19)$$

The balancing truncation as one of the methods for linear system model reduction gains popularity due to the property of easy use. Its aim is to find a transformation which makes reachability gramian and observability gramian diagonal and equal.

$$TPT^T = TQT^{-1} = \begin{bmatrix} \sigma_1 & & & & \\ & \sigma_2 & & & \\ & & \ddots & & \\ & & & \sigma_{n-1} & \\ & & & & \sigma_n \end{bmatrix}, \quad (20)$$

where σ is Hankel singular value and T is a transformation matrix. The Hankel singular values are ordered in magnitude in the diagonal line. Thus, the system is called in a balanced form. This state-space realization is called a balanced realization. The system is balancing in the following two senses [15]:

(i) P and Q are in a diagonal form; and

(ii) $P = Q$, which means that the relationship between the input-to-state behavior and the state-to-output behavior is balanced

From the Hankel singular value, it is clear to obtain the information that what states corresponding to the Hankel singular value contribute more or less to the system behavior than other states. So eliminate the states which have little effect on the system behavior and retain the states which influence input-output behavior at most, thus completing the work of model reduction.

It can be shown that there exists a state-space transformation

$$\bar{x} = Tx. \quad (21)$$

Such that the transformed system given by

$$\begin{cases} \dot{\bar{x}} = TAT^{-1}\bar{x} + TBu = \bar{A}\bar{x} + \bar{B}u \\ \bar{y} = CT^{-1}\bar{x} = \bar{C}\bar{x} \end{cases} \quad (22)$$

It is more interesting to point out that gramians act as a bridge between states and energy. The idea behind gramians is that the singular values in the controllability gramian correspond to the amount of energy applied to systems in order to steer the states to the expected place, and the singular values in the observability gramian refer to the energy generated by the corresponding states.

3.3. Optimal Placement Index. Gawronski has given the proofs for modes norm such as H_2 norm of a single mode, H_2 norm of a structure, H_∞ norm of a single mode, H_∞ norm of a structure, and H_2 and H_∞ hybrid norm of a single mode and a system [16]. H_2 and H_∞ hybrid norm of a single mode is expressed as follows:

$$\|G_i\|_{2,\infty} \cong \sqrt{\sum_{j=1}^r \|G_{i,j}\|_{(2,\infty)}^2}, \quad i = 1, \dots, n. \quad (23)$$

Index i regards the i th mode, and in the case of the norm for a whole structure, it should be omitted. Here, p represents the number of sensors. H_2 norm of the i th mode with a single sensor corresponding to the k th position is given by

$$\|G_i^k\|_2 = \frac{\|B_{mi}\|_2 \|C_{mi}^k\|_2}{2\sqrt{\zeta_i}\omega_i}. \quad (24)$$

Similarity, H_2 norm of the i th mode with a single sensor corresponding to the k th position is given by

$$\|G_i^k\|_\infty = \frac{\|B_{mi}\|_2 \|C_{mi}^k\|_2}{2\zeta_i\omega_i}. \quad (25)$$

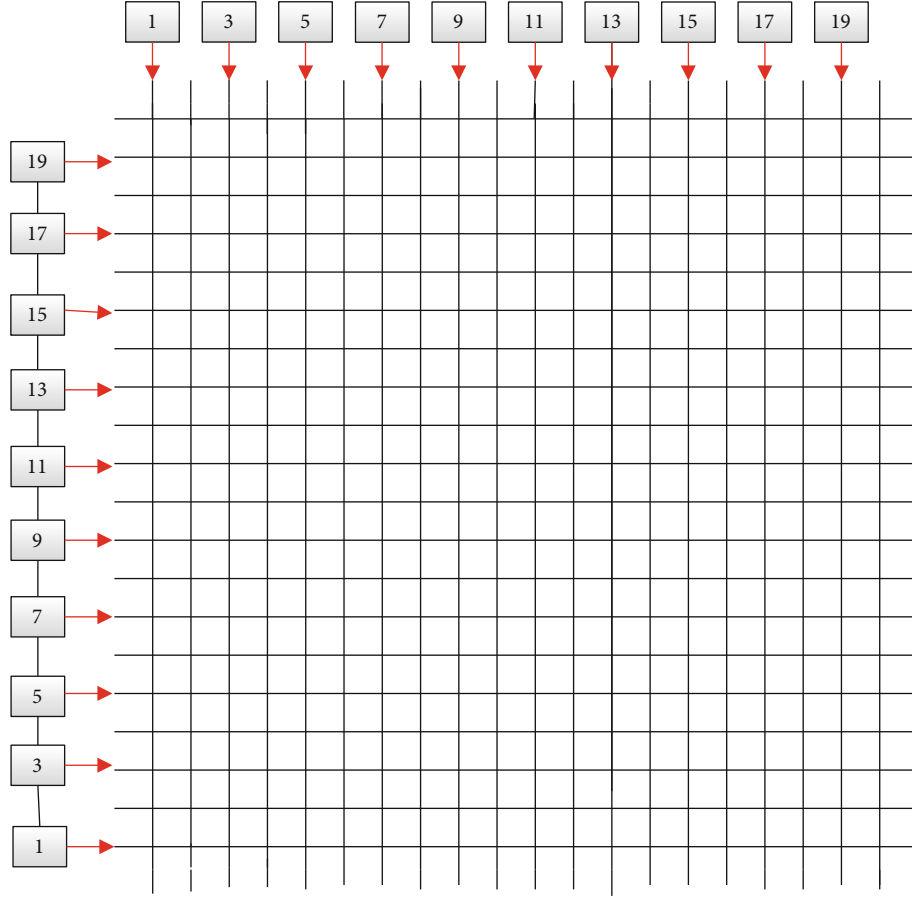


FIGURE 2: Candidate locations for sensors.

TABLE 1: . Candidate locations based on the largest placement indices.

Mode	H_2	H_∞	Observability index
1	(10,10)	(10,10)	(10,10)
2	(10,5), (10,6) (10,15), (10,16)	(10,5), (10,6) (10,15), (10,16)	(10,5), (10,6) (10,15), (10,16)
4	(10,4), (10,11), (10,18)	(10,4), (10,11), (10,18)	(10,4), (10,11), (10,18)
5	(5,6), (5,16) (15,6), (15,16)	(5,6), (5,16) (15,6), (15,16)	(5,6), (5,16) (15,6), (15,16)

The placement index is defined based on the H_2 norm and H_∞ norm. For a clear overview, the placement indices are arranged within appropriate placement matrices

$$N_{(2,\infty)} = \begin{bmatrix} \eta_1^1(2,\infty) & \eta_1^2(2,\infty) & \cdots & \eta_1^k(2,\infty) & \cdots & \eta_1^p(2,\infty) \\ \eta_2^1(2,\infty) & \eta_2^2(2,\infty) & \cdots & \eta_2^k(2,\infty) & \cdots & \eta_2^p(2,\infty) \\ \cdots & \cdots & \vdots & \cdots & \vdots & \cdots \\ \eta_i^1(2,\infty) & \eta_i^2(2,\infty) & \cdots & \eta_i^k(2,\infty) & \cdots & \eta_i^p(2,\infty) \\ \cdots & \cdots & \vdots & \cdots & \vdots & \cdots \\ \eta_n^1(2,\infty) & \eta_n^2(2,\infty) & \cdots & \eta_n^k(2,\infty) & \cdots & \eta_n^p(2,\infty) \end{bmatrix}, \quad (26)$$

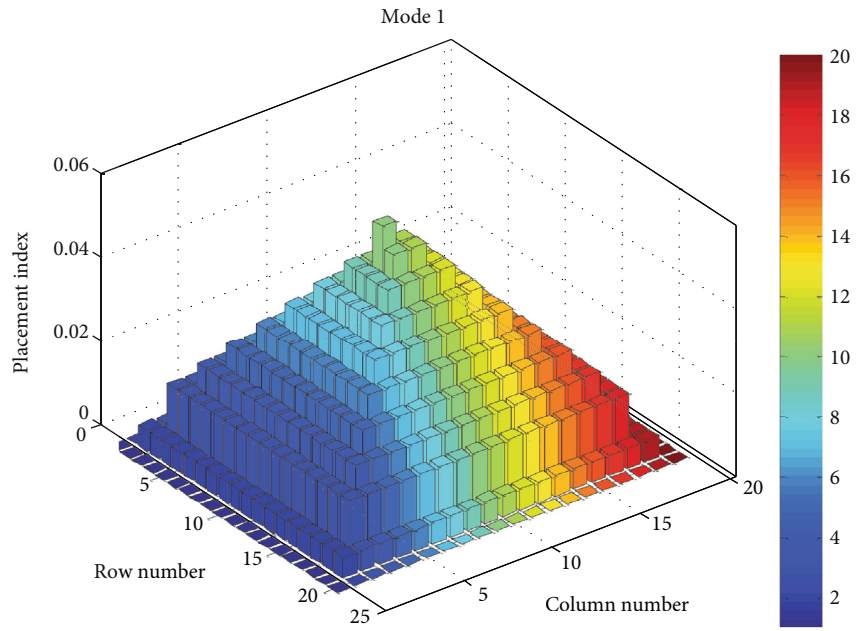
where each row corresponds to the i th mode and each column to the k th sensor. For the objective function in

terms of the H_2 norm, sensor (subscript s) placement indices are determined as the root mean square sum of the column-wise elements

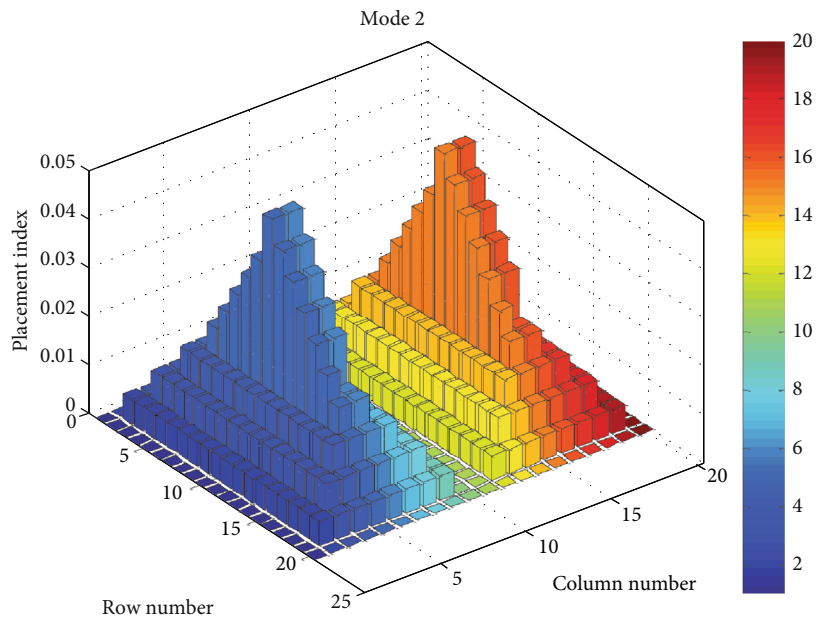
$$\eta_s^k = \sqrt{\sum_{i=1}^n (\eta_i^k)^2}, \quad k = 1, \dots, r. \quad (27)$$

For the objective function in terms of the H_∞ norm, the sensor placement index is the largest index over all modes

$$\eta_s^k = \max_i (\eta_i^k), \quad i = 1, \dots, n, \quad k = 1, \dots, r. \quad (28)$$

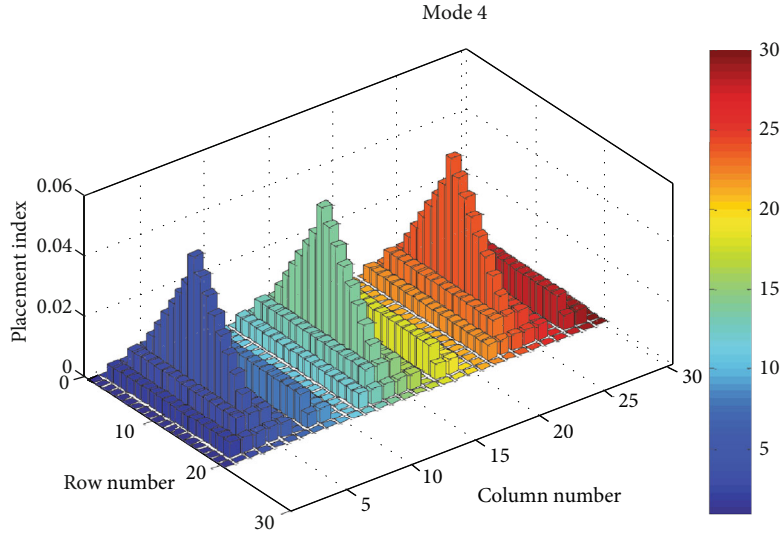


(a) Placement indices for mode 1

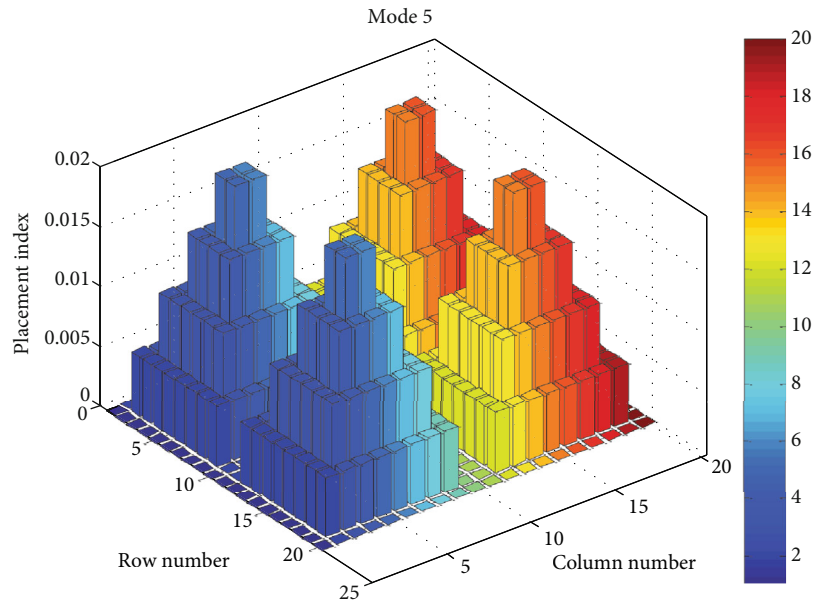


(b) Placement indices for mode 2

FIGURE 3: Continued.



(c) Placement indices for mode 4



(d) Placement indices for mode 5

FIGURE 3: Placement indices for the underground tunnel.

In order to draw comparison with the placement indices above, we introduce observability indices for the k th sensor location given by

$$v_i(k) = \frac{\varphi_i^T C_k^T C_k \varphi_i}{\varphi_i^T \varphi_i}. \quad (29)$$

The placement indices including H_2 norm placement indices, H_∞ norm placement indices, and observability indices provide guidelines for sensor deployment in the underground tunnel.

4. Optimal Sensor Placement in the Underground Tunnel

4.1. Mesh Generation of the Underground Tunnel. Shanghai underground tunnel belongs to shield tunnel. The sensor nodes are distributed on the ring segments with 20 m away between each two cross sections. There exists at least one routing node located on the cross section. The sink node is located outside the underground tunnel with the minimal average distance to each routing node, thus saving the energy consumption during data transportation process. According to the deployment principles, the grid cell of the underground tunnel cross section is obtained using mesh generation. Each grid cell represents the candidate location for the

sensor. The placement indices affect the deployment results. The meshing of the underground tunnel cross section is represented in Figure 2. Here, the corresponding rows and columns are numerated for a better preview.

4.2. Sensor Deployment in the Underground Tunnel. Each grid cell has its specific two-dimensional coordinate expressed by the row and the column shown in Figure 2. The placement indices of all grid cells are computed, and the corresponding largest values are selected to construct the table for candidate locations shown in Table 1. The simulation results of mode 3 are the same as those of mode 2. So the corresponding results of mode 3 are removed from Table 1.

It can be seen that qualitative representations of the placement indices based on H_2 and H_∞ hybrid norm as well as the observability index. The 3D bar diagrams of the placement indices based on the observability index are shown in Figure 3.

Each maximum placement index has the highest peak as shown in the 3D bar diagram. The grid cell corresponding to the highest peak is the optimal location for a sensor deployment. The optimal locations for sensor deployment are not the same under different modes. Moreover, the placement location has no relationship with mode order. It was found out that the placement condition is dominated by low order modes. Our research is limited to the first five modes.

It is noted that the probability that a node will be deployed in a candidate location where the placement index is equal to 1, regardless of nodes specific distributions such as Poisson distribution and exponential distribution.

5. Conclusion

In this paper, the optimization approaches for sensor node placement for the underground tunnel are proposed, based on balanced reduction of space state models. Based on H_2 and H_∞ norms, the optimal placement indices are obtained to determine optimal positions from many candidate locations. The pursuit of optimal position is crucial for sensor nodes to obtain maximal sensing information, thereby performing a good monitoring of the underground tunnel.

Data Availability

There is no data availability statement.

Conflicts of Interest

The authors declare that they have no conflicts of interest.

Acknowledgments

This work was supported by the National Natural Science Foundation of China (Grant No. 51875457).

References

- [1] M. R. Senouci, A. Mellouk, and K. Assnoute, "Localized movement-assisted sensor deployment algorithm for hole detection and healing," *IEEE Transactions on Parallel and Distributed Systems*, vol. 25, no. 5, pp. 1267–1277, 2014.
- [2] A. Nadeem, S. K. Salil, and J. Sanjay, "A pragmatic approach to area coverage in hybrid wireless sensor networks," *wireless communication and mobile computing*, vol. 11, no. 1, pp. 23–45, 2011.
- [3] C. Y. Chang, L. L. Huang, S. W. Chang, and Y. C. Chen, "Decentralized and energy-balanced algorithms for maintaining temporal full-coverage in full-coverage in mobile WSNs," *wireless communication and mobile computing*, vol. 12, no. 5, pp. 445–462, 2012.
- [4] L. A. Laranjeira and G. N. Rodrigues, "Border effect analysis for reliability assurance and continuous connectivity of wireless sensor networks in presence of sensor failures," *IEEE Transactions on Wireless Communications*, vol. 13, no. 8, pp. 4232–4246, 2014.
- [5] K. Kucuk and A. Kavak, "Connectivity analysis for wireless sensor networks with antenna array integrated central node," *wireless personal communications*, vol. 72, pp. 1361–1371, 2013.
- [6] S. B. He, J. M. Chen, and Y. X. Sun, "Coverage and connectivity in duty-cycled wireless sensor networks for event monitoring," *IEEE Transactions on Parallel and Distributed Systems*, vol. 23, no. 3, pp. 475–482, 2012.
- [7] C. Zhu, C. L. Zheng, L. Shu, and G. J. Han, "A survey on coverage and connectivity issues in wireless sensor networks," *Journal of Network and Computer Applications*, vol. 35, no. 2, pp. 619–632, 2012.
- [8] A. Chosh and S. K. Das, "Coverage and connectivity issues in wireless sensor networks: a survey," *Pervasive and Mobile Computing*, vol. 4, pp. 303–334, 2008.
- [9] A. Hada, K. Soga, R. Liu, and I. J. Wassell, "Lagrangian heuristic method for the wireless sensor network design problem in railway structural health monitoring," *Mechanical System and Signal Processing*, vol. 28, pp. 20–35, 2012.
- [10] C. Hirai and K. Soge, "An experimental model of relay development planning tool for wireless sensor network system to monitor civil engineering structure," *Proceeding of the 19th LASTED International Conference Parallel and Distributed Computing and Network (PDCN 2010)*, 2010, pp. 164–171, Innsbruck, Austria, 2010.
- [11] V. Gupta, M. Sharma, and N. Thakur, "Optimization criteria for optimal placement of piezoelectric sensors and actuators on a smart structure: a technical review," *Journal of Intelligent Material Systems and Structures*, vol. 21, no. 12, pp. 1227–1243, 2010.
- [12] T. Nestorovic and M. Trajkov, "Optimal actuator and sensor placement based on balanced reduced models," *Mechanical Systems and Signal Processing*, vol. 36, no. 2, pp. 271–289, 2013.
- [13] S. Meguerdichian, K. Koushanfar, G. Qu, G. Veltri, and M. Potkonjak, "Exposure in wireless sensor networks: theory and practical solutions," *Wireless Networks*, vol. 8, no. 5, pp. 443–454, 2002.
- [14] B. C. Moore, "Principal component analysis in linear systems: controllability, observability, and model reduction," *IEEE Transaction on Automatic Control*, vol. 26, no. 1, pp. 17–32, 1981.
- [15] K. Fujimoto and J. M. A. Scherpen, "Balanced realization and model order reduction for nonlinear systems based on singular value analysis," *SIAM Journal on Control and Optimization*, vol. 48, no. 7, pp. 4591–4623, 2010.
- [16] W. Gawronski, *Advanced Structural Dynamics and Active Control of Structures*, Springer, New York, 2004.